MODELING AND ANALYSES OF PRETWISTED BEAMS HAVING PIEZOELECTRIC SMART MATERIALS

A Thesis Submitted to
the Graduate School of Engineering and Sciences of
İzmir Institute of Technology
in Partial Fulfillment of the Requirements for the Degree of

MASTER OF SCIENCE

in Mechanical Engineering

by
Merve AKARİ

December 2017
İZMİR

We approve the thesis of **Merve AKARİ**

Examining Committee Members:

Prof. Dr. Bülent YARDIMOĞLU
Department of Mechanical Engineering, İzmir Institute of Technology

Prof. Dr. Serhan ÖZDEMİR
Department of Mechanical Engineering, İzmir Institute of Technology

Prof. Dr. Zeki KIRAL
Department of Mechanical Engineering, Dokuz Eylül University

27 December 2017

Prof. Dr. Bülent YARDIMOĞLU
Supervisor, Department of Mechanical Engineering,
İzmir Institute of Technology

Prof. Dr. Metin TANOĞLU
Head of the Department of
Mechanical Engineering

Prof. Dr. Aysun SOFUOĞLU
Dean of the Graduate School
of Engineering and Sciences

ACKNOWLEDGEMENTS

I would like to express my special gratitude and thanks to my adviser Prof. Dr. Bulent YARDIMOGLU who spent his time for me and give me consistent advice , helped me bring this study into reality.

Foremost I would like to dedicate this thesis to my mother Seher OZER who has a strong and gentle soul, encouraging me to trust myself, believe in hard work, and so much could be done with little sources.

It is my privilege to thank my kiddie Hebrid, for his dynamism have enabled me for finished my responsibilities.

I thank profusely and extend my appreciations also go to Faruk Ekiz for being my guardian during my educational career.

ABSTRACT

MODELING AND ANALYSES OF PRETWISTED BEAMS HAVING PIEZOELECTRIC SMART MATERIALS

In this study, modeling and analyses of pretwisted beams having piezoelectric smart materials are acomplished by using Finite Element Method. A computer program is developed by using APDL (ANSYS Parametric Design Language) in ANSYS with SOLID45 and SOLID5 for pretwisted beam and piezoelectric layer, respectively. The effects of the pretwist angle on electric field are analyzed.

ÖZET

PİEZOELEKTRİK AKILLI MALZEMEYE SAHİP ÖNBURULMALI ÇUBUKLARIN MODELLENMESİ VE ANALİZLERİ

Bu çalışmada, piezoelektrik akıllı malzemeleri içeren ön burulmalı kirişlerin modellenmesi ve analizi, Sonlu Elemanlar Yöntemi kullanılarak gerçekleştirilmiştir. İlk olarak, önburulmalı kiriş ve piezoelektrik tabaka için ANSYS'de APDL (ANSYS Parametrik Tasarım Dili) de SOLID45 ve SOLID5 kullanılarak bir bilgisayar programı geliştirilmiştir. Önburulma açısının elektrik alanı üzerindeki etkileri analiz edilmiştir.

TABLE OF CONTENTS

LIST OF FIGURES

Figure **Page**

LIST OF TABLES

Table **Page**

LIST OF SYMBOLS

b	Breadth of the beam
b_p	Breadth of the piezoelectric patch
$[B_u]$	Strain-displacement matrix
$[B_V]$	Electrical field-electrical potential matrix
c	Young's modulus
d	Piezoelectric strain coefficient
d_p	Distance of the piezoelectric patch from the fixed support
D	Dielectric displacement
e	Electric displacement and strain relationship
EI	Bending rigidity
E	Modulus of elasticity, Electric field
$\{F\}$	Nodal force vector
h	Height of the beam
I_{xx}, I_{yy}	Area moments of inertia of the cross-section about *xx* and *yy* axes
I_{xy}	Product moment of inertia of the cross-section about *xx*-*yy* axes
$I_{x'x'}$, $I_{y'y'}$	Area moments of inertia of the cross-section about *x'x'* and *y'y'* axes
k	Coupling coefficient of piezoelectric material
$[K]$	Structural stiffness matrix
$[K_d]$	Dielectric conductivity
$[K_z]$	Piezoelectric coupling matrix
L	Length of the beam
$\{L\}$	Nodal change vectors
M_x, M_y	Bending moments about *x* and *y* axes
$[N^u]$	Shape function matrix for displacements
n	Number of disks in the stack
N_i	Shape function for node *i*
s	Inverse of Young's modulus
s^E	s in constant electric field
s_p	Length of the piezoelectric patch

S	Strain
t_p	Thickness of the piezoelectric patch
T	Stress
u	Linear displacement in xz plane
$\{u\}$	Nodal displacement vector
$\{u_c\}$	Displacement vector
U	Voltage
v	Linear displacement in yz plane
$\{V\}$	Nodal electric potential vector
vol	Volume
V_c	Electric potential
x , y	Principal axes through the centroid at root section
x' , y'	Principal axes through the centroid at any section
z	Co-ordinate distance measured along beam
δ	Displacement of tip of the beam
ε	Dielectric permittivity
ε^T	ε in constant stress
ε^S	ε in constant strain
ϕ_0	Initial pretwist angle of the finite element
ϕ	Pretwist angle of the finite element at any section
θ	Twist angle per unit length

CHAPTER 1

GENERAL INTRODUCTION

Pretwisted beams may have symmetrical or unsymmetrical cross-sections in local coordinates. If it is symmetrical in its local coordinate, bending deformations of pretwisted beam in two planes are coupled.

On the other hand, if the cross-section of the pretwisted beam is not symmetric in its local coordinate, then torsional deformation is also coupled with the two bending deformations. Similar to previous statement, it is called bending-bending-torsion coupling. Many investigators studied on the pretwisted beams. Some of them are presented in the next paragraphs.

Houbolt and Brooks (1958) developed the differential equations for the lateral and torsional deformations of twisted rotating beams and used a Rayleigh-Ritz approach to compute the solution. Their model is illustrated in Figure 1.1.

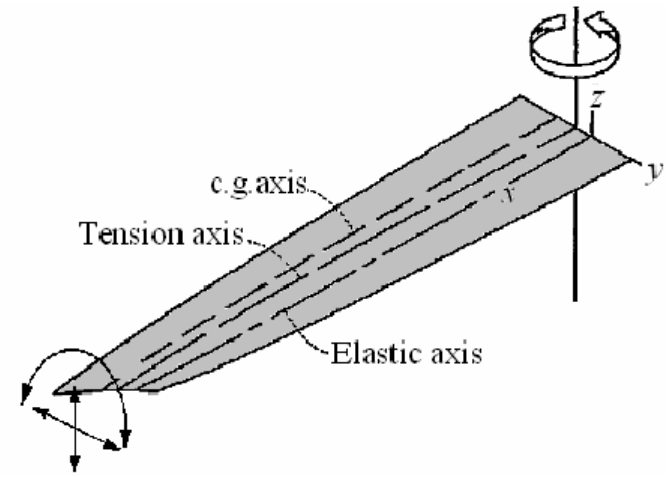

Figure 1.1. Twisted rotating beam
(Source: Houbolt and Brooks 1958)

Montoya (1966) derived the equations of motion for a rotating pre-twisted cantilever beam with an aerofoil cross-section shown in Figure 1.2. He included shear center and higher order effects, and solved these by Runge-Kutta method. He performed experimental studies for verification of his theoretical approach.

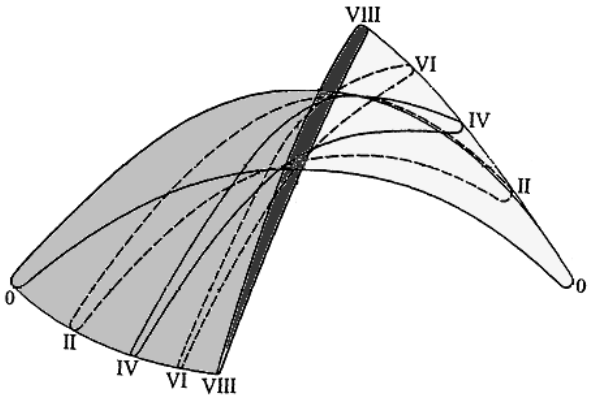

Figure 1:2. Twisted beam with aerofoil cross-section
(Source: Montoya 1966)

Fu (1974) studied on rotating pre-twisted non-uniform Timoshenko beam having coupled bending-bending-torsion vibration by using a set of recursion formulas as the basis of a lumped parameter approach.

Recently, Yardimoglu and Inman (2004) proposed a finite element model having fourteen degrees of freedom for coupled bending-bending-torsion vibration of a rotating pre-twisted thick beam with varying aerofoil cross-section.

One of the earliest papers on smart materials for vibration control is that of Bailey and Hubbard (1985). They described the use of piezoelectric materials to control the vibration of a beam. Their study has been cited 491 times up to now. Another seminal work in the field of smart materials is a paper by Crawley and de Luis (1987).

There are various textbooks on the subject of smart materials. Some of them were written by Preumont (2002), Smith (2005), Leo (2007), and Ganguli et al (2016).

Cesnik and Morales (2001) presented a finite-element analysis of pretwisted and curved active composite beams with embedded anisotropic actuation. They approximated the 3-D beam problem to 1-D one by considering the certain small parameters in the modeling.

Song et al (2002) modeled pretwisted thin-walled beams with piezo actuators bonded or embedded into the structure for dynamic behavior under adaptive capabilities.

Shete et al (2007) analyzed the optimal control of a pretwisted smart composite rotating single-celled box beam having transverse shear flexibility. They underscored that shear strain variation across the beam wall for achieving efficient control is important.

Choi et al (2007) interested in bending vibration control of the rotating pretwisted thin-walled beam with piezoelectric fiber composites. They used finite element method for numerical studies and applied a negative velocity feedback control algorithm. Their investigation focused on determination of the effects of design parameters of beams such as rotating speeds, pretwist angles and fiber orientations on active vibration control.

Liu et al (2007) derived the governing equations and boundary conditions for extension, torsion, and cross-sectional warping of pretwisted beams by using the semi-inverse method and Hamilton's principle and investigated the resonance frequencies analytically.

Kiral et al (2008) studied on active vibration control and residual vibrations of a cantilever smart beam. They used finite element method in order to design a suitable control technique and they verified their results by experiments.

Valliappan et al (2014) developed a model of initially-curved and pre-twisted smart beam and used the Variational Asymptotic Method (VAM).

Wang et al (2015) studied on coupled flexural–torsional vibration of spinning smart beams with asymmetric cross-sections considering the warping effect. They used distributed piezoelectric sensor and actuator layers to control the vibration of the spinning beam which has not constant natural characteristics due to the spinning velocity. The positive position feedback (PPF) approach is employed for control algoritm.

In this study, modeling and analyses of pretwisted beams having piezoelectric smart materials are acomplished by using Finite Element Method. A computer program is developed by using APDL (ANSYS Parametric Design Language) in ANSYS with SOLID45 and SOLID5 for pretwisted beam and piezoelectric layer, respectively. The effects of the pretwist angle on electric field are analyzed.

CHAPTER 2

THEORETICAL STUDIES

2.1. Introduction

In this chapter, the geometrical properties of pretwisted beam are given mathematically with illustration for the next sections in the following section. Differential equations of pretwisted beam are introduced. Then, piezoelectric materials are explained and its constitutive equations are summarized. Differential equations of pretwisted beam are extended for piezoelectric patch effect on the system. As numerical solution procedure, finite element method is presented. Finally, modeling and analysis in ANSYS is outlined.

2.2. Geometrical Properties of Pretwisted Beam

The pretwisted beam in this study is given in Figure 2.1. It is seen from Figure 2.1 that it has rectangular cross-section. Also, the cross-section of the pretwisted beam is uniform along the z axis, except its rotation about *z* axis.

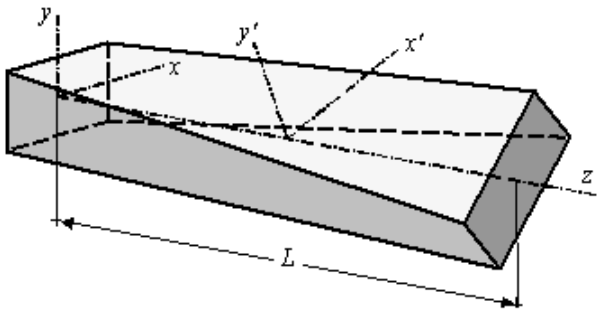

Figure 2.1. The geometry of pretwisted beam

The second moments of cross-sectional area based on the co-ordinate system shown in Figure 2.1 are given by Yardimoglu and Yildirim (2004) as follows

$$I_{xx}(z) = I_{x'x'}\cos^2\phi(z) + I_{y'y'}\sin^2\phi(z) \tag{2.1}$$

$$I_{yy}(z) = I_{y'y'}\cos^2\phi(z) + I_{x'x'}\sin^2\phi(z) \tag{2.2}$$

$$I_{xy}(z) = 0.5\left(I_{y'y'} - I_{x'x'}\right)\sin 2\phi(z) \tag{2.3}$$

where

$$\phi(z) = \phi_0 + \theta z \tag{2.4}$$

Equation (2.4) states that pretwist of the beam along the z axis is linear.

2.3. Differential Equations of Pretwisted Beam

The Bernoulli-Euler beam theory is extended for mathematical model of the pretwisted beam shown in Figure 2.1. The differential equations of a pretwisted beam for coupled bending-bending displacement can be written as (Yardimoglu, 2016)

$$EI_{xx}(z)v'' + EI_{xy}(z)u'' = M_x(z) \tag{2.5}$$

$$EI_{yy}(z)u'' + EI_{xy}(z)v'' = M_y(z) \tag{2.6}$$

where E is the modulus of elasticity of the beam material, $I_{xx}(z)$, $I_{yy}(z)$, and $I_{xy}(z)$ are the second moments of cross-sectional area which are defined in Equations (2.1) to (2.3), respectively. Also, $M_x(z)$ and $M_y(z)$ are external moment functions applied to pretwisted beam about x and y axis, respectively.

2.4. Piezoelectric Materials

In 1880, Pierre and Jacques Curie discovered the direct piezoelectric effect which is illustrated in Figure 2.2. This effect is based on the generation of stress due to the current applied to piezoelectric material which is produced by poling (aligning) of the material as shown in Figure 2.3. This is accomplished by heating the material above its Curie temperature and applying a strong electric field. The Curie temperature is the minimum temperature to arrange electric dipoles from random direction to applied electric field direction (Ganguli et al 2016).

Converse piezoelectric effect is illustrated in Figure 2.2. It can be seen from this figure that the cause and effect in the direct piezoelectric effect are switched, namely, piezoelectric material under the electric field produces stress.

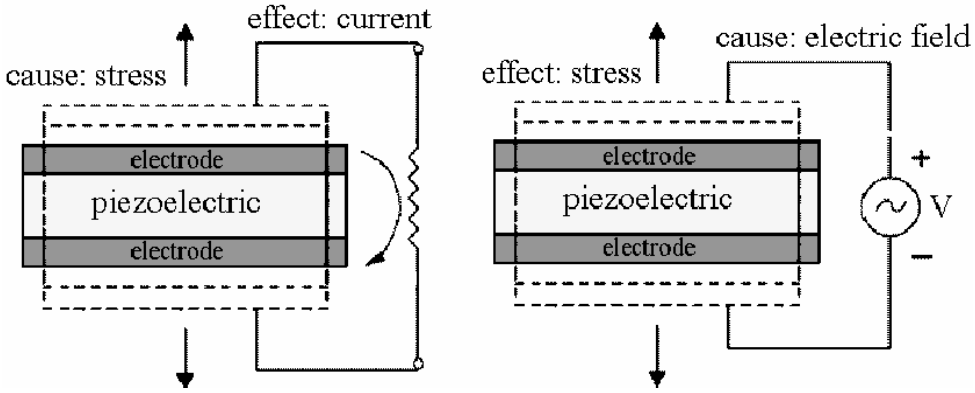

Figure 2.2. Direct and converse piezoelectric effect
(Source: Ganguli et al 2016)

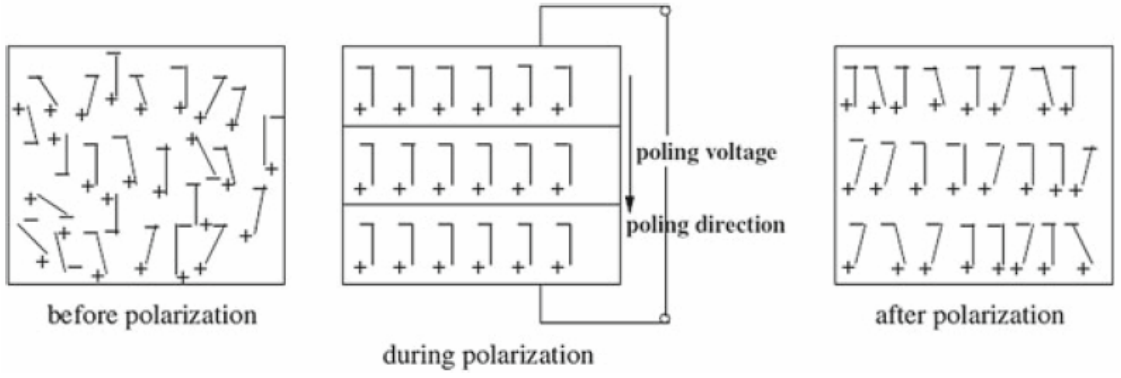

Figure 2.3. Polarization process
(Source: Ganguli et al 2016)

2.5. Constitutive Equations of Piezoelectric Materials

The equations and notations used in this section are based on the excellent textbook on smart material systems written by Leo (2007). His textbook has the nomenclature stated in the IEEE Standard on Piezoelectricity (1988).

In order to simplify the presentation of the constitutive equation of piezoelectric materials, one dimensional model is selected as first step.

Mechanical stress and electrical displacement are coupled in piezoelectric materials. In other words, if mechanical stress is applied to piezoelectric materials, it produces an electrical displacement, and vice versa. Because of this property, it is used for sensing and actuation.

The mechanical-to-electrical coupling is called as the direct effect, while the electrical-to-mechanical coupling is known as the converse piezoelectric effect.

In *direct piezoelectric effect*, the stress T (N/m^2) which applied to piezoelectric materials gives two results: strain S (m/m) and electric displacement D (C/m^2) as follows:

$$S = \frac{1}{Y} T = s\, T \tag{2.7}$$

where s (m^2/N) is the reciprocal of the modulus which is called the mechanical compliance and

$$D = d\, T \tag{2.8}$$

where d (C/N) is the piezoelectric strain coefficient.

In *converse piezoelectric effect*, the electric field E (V/m) which applied to piezoelectric materials gives again the same two results as follows:

$$S = d\, E \tag{2.9}$$

where d (m/V) is the piezoelectric strain coefficient and

$$D = \varepsilon E \tag{2.10}$$

where ε (F/m) is dielectric permittivity of the material.

Equations (2.7) to (2.10) can be combined into a matrix form as

$$\begin{Bmatrix} S \\ D \end{Bmatrix} = \begin{bmatrix} s & d \\ d & \varepsilon \end{bmatrix} \begin{Bmatrix} T \\ E \end{Bmatrix} \tag{2.11}$$

Equation (2.11) can be expressed with strain and electric displacement as the independent variables as

$$\begin{Bmatrix} T \\ E \end{Bmatrix} = \frac{1}{s\varepsilon - d^2} \begin{bmatrix} \varepsilon & -d \\ -d & s \end{bmatrix} \begin{Bmatrix} S \\ D \end{Bmatrix} \tag{2.12}$$

or

$$\begin{Bmatrix} T \\ E \end{Bmatrix} = \frac{1}{1 - k^2} \begin{bmatrix} s^{-1} & -d^{-1}k^2 \\ -d^{-1}k^2 & \varepsilon^{-1} \end{bmatrix} \begin{Bmatrix} S \\ D \end{Bmatrix} \tag{2.13}$$

where k is called the piezoelectric coupling coefficient and given as

$$k = \frac{d}{\sqrt{s\varepsilon}} \tag{2.14}$$

It is possible to generalize the equations presented above for the case of an arbitrary volume of piezoelectric material. For this purpose, the piezoelectric material with coordinate system illustrated in Figure 2.4 is considered.

A general three dimensional piezoelectric material is characterized by 36 independent elastic constants, 18 piezoelectric strain coefficients, and 9 dielectric permittivity values. Therefore, there are 63 coefficients for stress, strain, electric field, and electric displacement. However, the many common piezoelectric materials have orthotropic properties. Therefore, the numbers of coefficients required for the constitutive properties of piezoelectric materials are reduced significantly.

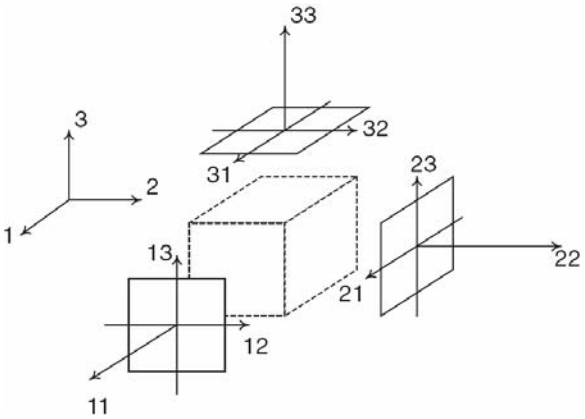

Figure 2.4. The coordinate axes of the three-dimensional piezoelectric cube (Source: Leo 2007)

The constitutive equations of piezoelectric material having aforementioned properties are given as follows:

$$\begin{Bmatrix} S_1 \\ S_2 \\ S_3 \\ S_4 \\ S_5 \\ S_6 \end{Bmatrix} = \begin{bmatrix} s_{11} & s_{12} & s_{13} & 0 & 0 & 0 \\ s_{12} & s_{22} & s_{23} & 0 & 0 & 0 \\ s_{13} & s_{23} & s_{33} & 0 & 0 & 0 \\ 0 & 0 & 0 & s_{44} & 0 & 0 \\ 0 & 0 & 0 & 0 & s_{55} & 0 \\ 0 & 0 & 0 & 0 & 0 & s_{66} \end{bmatrix} \begin{Bmatrix} T_1 \\ T_2 \\ T_3 \\ T_4 \\ T_5 \\ T_6 \end{Bmatrix} + \begin{bmatrix} 0 & 0 & d_{13} \\ 0 & 0 & d_{23} \\ 0 & 0 & d_{33} \\ 0 & d_{24} & 0 \\ d_{15} & 0 & 0 \\ 0 & 0 & 0 \end{bmatrix} \begin{Bmatrix} E_1 \\ E_2 \\ E_3 \end{Bmatrix} \tag{2.15}$$

$$\begin{Bmatrix} D_1 \\ D_2 \\ D_3 \end{Bmatrix} = \begin{bmatrix} 0 & 0 & 0 & 0 & d_{15} & 0 \\ 0 & 0 & 0 & d_{24} & 0 & 0 \\ d_{13} & d_{23} & d_{33} & 0 & 0 & 0 \end{bmatrix} \begin{Bmatrix} T_1 \\ T_2 \\ T_3 \\ T_4 \\ T_5 \\ T_6 \end{Bmatrix} + \begin{bmatrix} \varepsilon_{11} & 0 & 0 \\ 0 & \varepsilon_{22} & 0 \\ 0 & 0 & \varepsilon_{33} \end{bmatrix} \begin{Bmatrix} E_1 \\ E_2 \\ E_3 \end{Bmatrix} \tag{2.16}$$

The polarization vector of piezoelectric materials is aligned in the direction of 3 axis. The common operating modes of piezoelectric transducers for use as sensors or actuators are 33 and 31. Second number in the operating mode refers to direction of strain.

The multilayer piezoelectric stack shown in Figure 2.5 is an example for 33 operating mode. Figure 2.6 shows a bimorph piezoelectric beam for 31 operating mode.

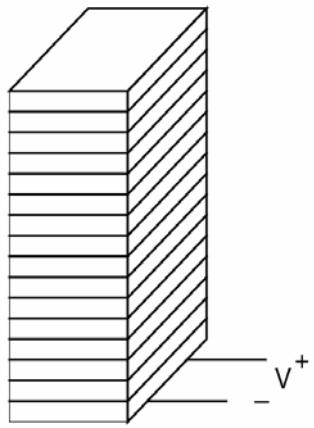

Figure 2.5. The multilayer piezoelectric stack
(Source: Leo 2007)

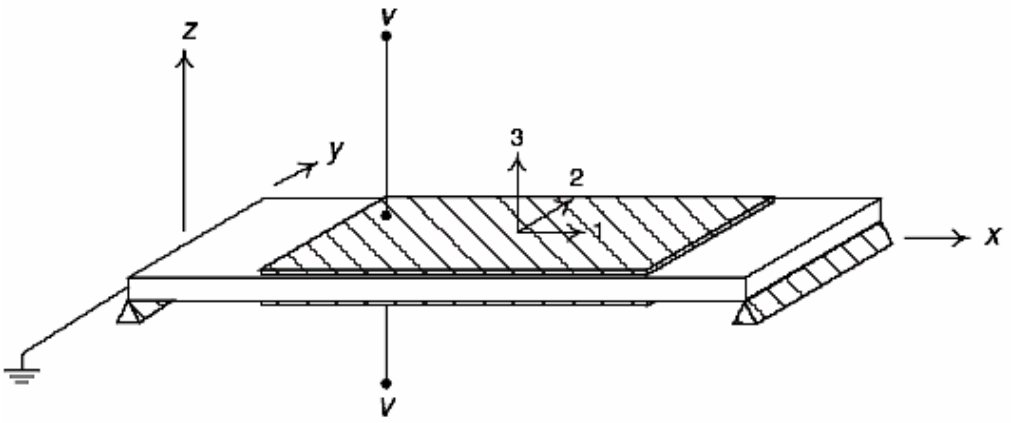

Figure 2.6. A pinned–pinned bimorph piezoelectric beam
(Source: Leo 2007)

For 33 operating mode, $T_1=T_2=T_4=T_5=T_6=E_1=E_2=0$ can be assumed. Also, S_1 and S_2 are not main interest. Therefore, the following constitutive equations are needed

$$S_3 = \frac{1}{Y_3^E} T_3 + d_{33} E_3 \tag{2.17}$$

where Y_3^E is the Young's modulus of the material in the 3 direction for the constant electric field which denoted by superscript *E*.

$$D_3 = d_{33}T_3 + \varepsilon_{33}^T E_3 \tag{2.18}$$

where the superscript *T* denotes a stress-free (*T*=0) condition.

Similar to 33 operating mode, 31 operating mode can be based on assumption $T_2=T_3= T_4=T_5=T_6=E_1=E_2=0$. Also, S_2 and S_3 are not main interest. Thus, the following constitutive equations are required

$$S_1 = \frac{1}{Y_1^E}T_1 + d_{13}E_3 \tag{2.19}$$

$$D_3 = d_{13}T_1 + \varepsilon_{33}^T E_3 \tag{2.20}$$

2.6. Differential Equations of Smart Pretwisted Beam

The differential equations of pretwisted beam are presented in Section 2.3 by Equations (2.5) and (2.6) for the applied moments effects $M_x(z)$ and $M_y(z)$.

When a thin piezoelectric material is fixed to lateral surface of the beam, it causes bending moment for this beam, if it is under electric field. Therefore, these bending moments can be treated as a part of applied moments.

$$M_x(z) = M_{ex}(z) + M_p E_3 \tag{2.21}$$

$$M_y(z) = M_{ey}(z) + M_p E_3 \tag{2.22}$$

where $M_{ex}(z)$ and $M_{ey}(z)$ are the moment applied by external loads and M_p is the moment applied by the piezoelectric layers per unit electric field (N.m/(V/m)) which can be written as follows

$$M_p = z_G F_p \tag{2.23}$$

where z_G is the centroid of the piezoelectric layers with respect to neutral axis of the beam shown in Figure 2.7 and F_p is the force applied by the piezoelectric layers per unit electric field which is calculated from the following equation

$$F_p = d_{13} E_p A_p \tag{2.24}$$

where A_p is the cross-sectional area of the piezoelectric layer.

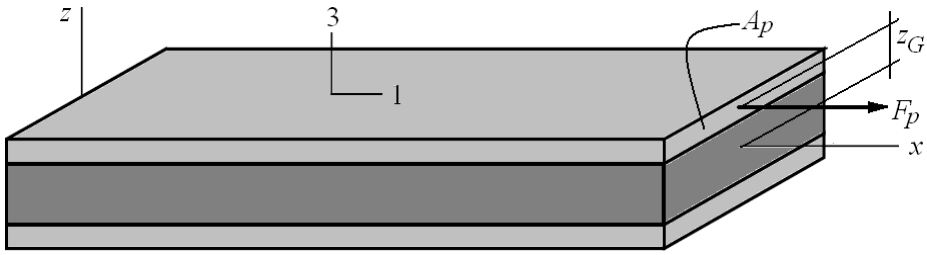

Figure 2.7. The force applied by the piezoelectric layer

2.7. Finite Element Method

Finite element method is generalized form of Rayleigh-Ritz method (Reddy 1993, Petyt 2010) and has been developed before half century ago (Cook 1989). In this method, nonuniform domain is divided into uniform small bodies such as in the shape of bar, beam, plate, and shell, in order to model the main nonuniform domain. These small bodies are called as finite element which has connecting points with its neighbors that are called nodes. Therefore, domain parameters are discretized in nodes. Division process is known as meshing.

If the problem is related with solid mechanics, characteristic matrix of the body is the stiffness matrix and nodal freedoms are displacements as linear and angular. Modeling of the whole domain is completed by assembling the all finite element and applying the boundary condition.

Selecting of the types and determination of the size of the finite element is the most critical steps for modeling. Moreover, selecting the numerical method in the commercial finite element packages requires backgrounds for these methods to get the solution accurately (Yardimoglu, 2015).

2.8. Modeling and Analysis in ANSYS

The constitutive equations for finite element formulation is given by Allik and Hughes (1970) which are used and cited in Kohnke (2004) as

$$\{T\} = [c]\{S\} - [e]\{E\} \tag{2.25}$$

$$\{D\} = [e]^T\{S\} + [\varepsilon]\{E\} \tag{2.26}$$

where $\{T\}$, $\{D\}$, $\{S\}$, and $\{E\}$ are stress, electric flux density, mechanical strain, and electric field vectors, respectively. Also, $[c]$, $[e]$, and $[\varepsilon]$ are the elastic stiffness matrix evaluated at constant electric field, the piezoelectric matrix and the dielectric matrix evaluated at constant mechanical strain, respectively.

The two coupled equilibrium equations in finite element domain which are used in Kohnke (2004) are given by Allik and Hughes (1970) as

$$\begin{bmatrix} [K] & [K^z] \\ [K^z]^T & [K^d] \end{bmatrix} \begin{Bmatrix} \{u\} \\ \{V\} \end{Bmatrix} = \begin{Bmatrix} \{F\} \\ \{L\} \end{Bmatrix} \tag{2.27}$$

where $[K]$, $[K^d]$, and $[K^z]$ are structural stiffness, dielectric conductivity, and piezoelectric coupling matrices, respectively. These matrices are described in Kohnke (2004) as follows

$$[K] = \iiint_{vol} [B_u]^T [c][B_u] dvol \tag{2.28}$$

$$[K^d] = \iiint_{vol} [B_V]^T [\varepsilon][B_V] dvol \tag{2.29}$$

$$[K^z] = \iiint_{vol} [B_u]^T [e][B_V] dvol \tag{2.30}$$

in which $[B_u]$ and $[B_V]$ are defined in Kohnke (2004).

$\{u\}$ and $\{V\}$ in Equation (2.27) are the nodal displacements and nodal electrical potential vectors, respectively. They are written in open form as

$$\{u\} = \{Ux_1 \quad Uy_1 \quad Uz_1 \quad \cdots \quad Ux_n \quad Uy_n \quad Uz_n\}^T \tag{2.31}$$

$$\{V\} = \{V_1 \quad V_2 \quad \cdots \quad V_n\}^T \tag{2.32}$$

The right hand side terms in the Equation (2.27): $\{F\}$ and $\{L\}$ are nodal force and nodal charge vectors, respectively. They are input values of the model.

The strain vector $\{S\}$ is expressed in terms of the displacement vector $\{u\}$ as

$$\{S\} = [B_u]\{u\} \tag{2.33}$$

On the other hand, the electric field vector {E} is expressed in terms of the electrical potential vector $\{V\}$ as

$$\{E\} = -[B_V]\{V\} \tag{2.34}$$

Having the nodal displacement and electric potential for an element from solution of Equation (2.27), the stresses and the electric flux density at any point within the finite element are obtained by substituting Equations (2.33) and (2.34) into Equations (2.25) and (2.26) as

$$\{T\} = [c][B_u]\{u\} + [e][B_V]\{V\} \tag{2.35}$$

$$\{D\} = [e]^T[B_u]\{u\} - [\varepsilon][B_V]\{V\} \tag{2.36}$$

The finite element model of the smart pretwisted beam is modeled in ANSYS by employing SOLID45 and SOLID5 for pretwisted beam and piezoelectric layer, respectively. A computer program is developed by using APDL (ANSYS Parametric Design Language) in ANSYS.

CHAPTER 3

NUMERICAL STUDIES

3.1. Verification of Finite Element Model

The uniform rectangular cross-sectioned pretwisted beam having breadth b, height h, length L, total twist angle θ at its free end is parametrically modeled in ANSYS as shown in Figure 3.1 for the numerical data b=20 mm, h=2 mm, L=300 mm, θ=-45º.

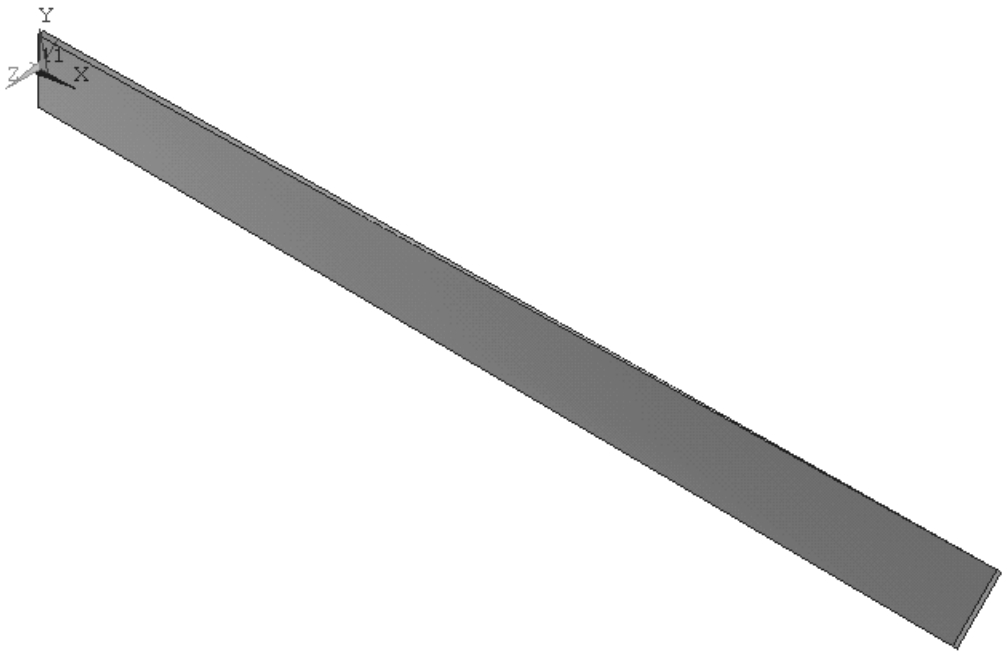

Figure 3.1 Geometrical model of the pretwisted beam

After geometric modeling of the pretwisted beam, it is meshed by SOLID45 in ANSYS which gives the numerical results in the analysis as possible as near to theoretical results. For this purpose, untwisted form of the beam is considered to determine the number of element which is necessary for desired accuracy in results. Therefore, its untwisted form is obtained in ANSYS by setting θ=0º as shown in Figure 3.2.

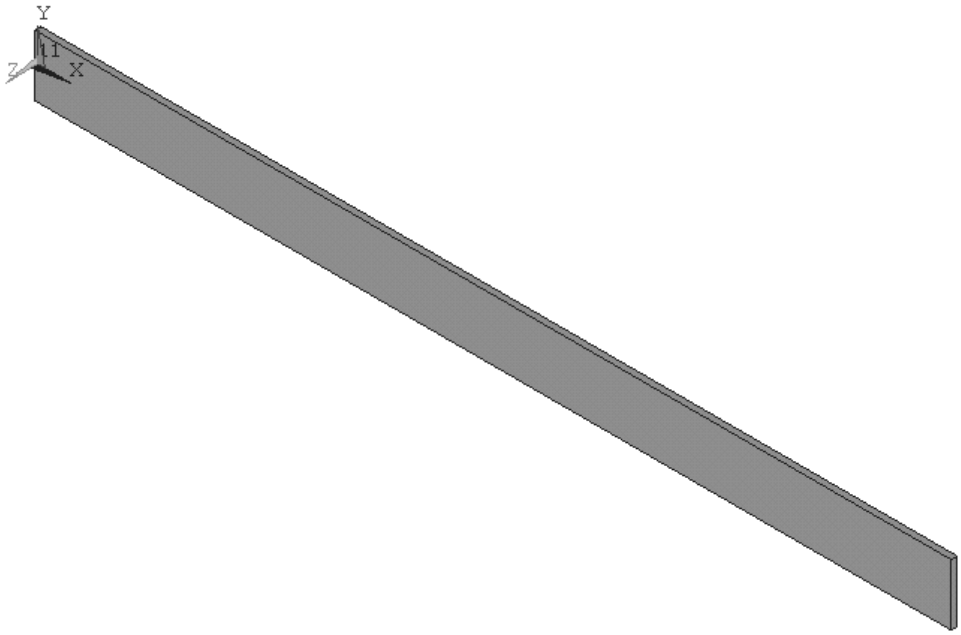

Figure 3.2 Geometrical model of the untwisted beam

The fixed-free boundary condition is applied to the geometrical model shown in Figure 3.2. It is meshed with different number of SOLID45 elements and loaded from its tip point on neutral axis by a force F_z acting in -z direction, in order to decide for the meshing parameters comparing the displacement of tip point with the analytical result.

Selecting the tip force F_z=0.5 N and finding the tip displacements for usage of different number of finite elements, mesh parameters are determined as follows:

- number of elements in x direction = 60,
- number of elements in y direction = 4,
- number of elements in z direction = 1.

Displacement of the tip point of the cantilever beam for the determined mesh parameters and analytical results based on aluminum of which modulus of elasticity E=62 GPa are given in Table 3.1. Finite element model of the fixed-free untwisted beam under tip load is shown in Figure 3.3.

Table 3.1. Displacements of tip point (m)

Analytical by $\delta=F_zL^3/3EI$	0.00544
Numerical by FEM	0.00540

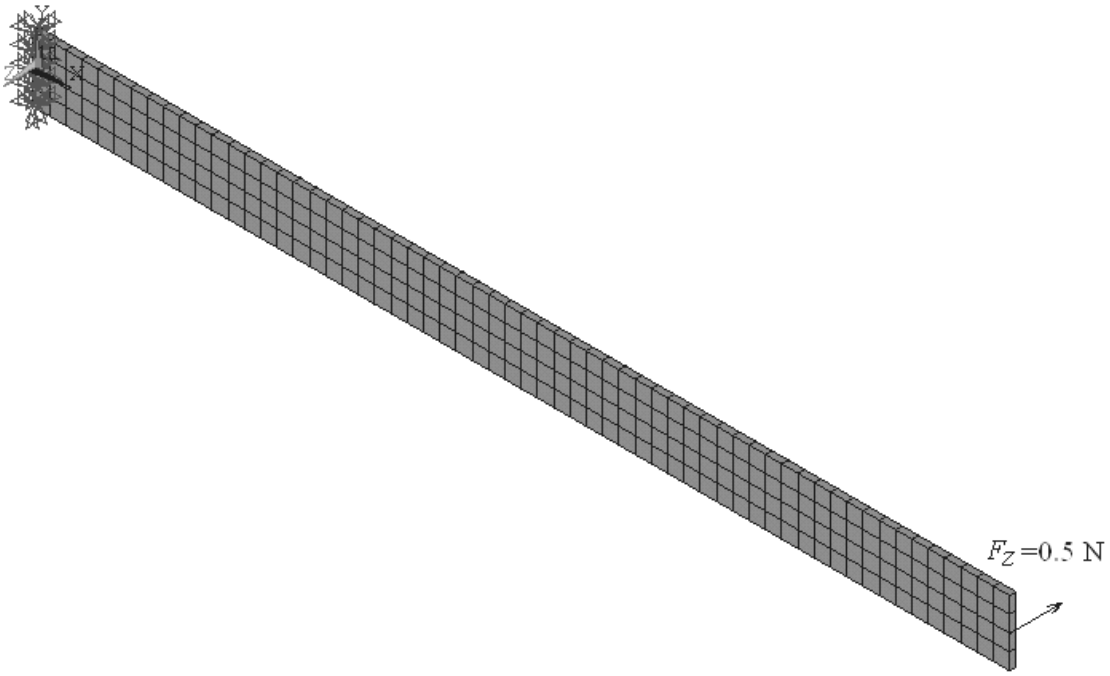

Figure 3.3 Finite element model of the fixed-free untwisted beam under tip load

Also, deformed and undeformed states of the fixed-free untwisted beam is illustrated in Figure 3.4.

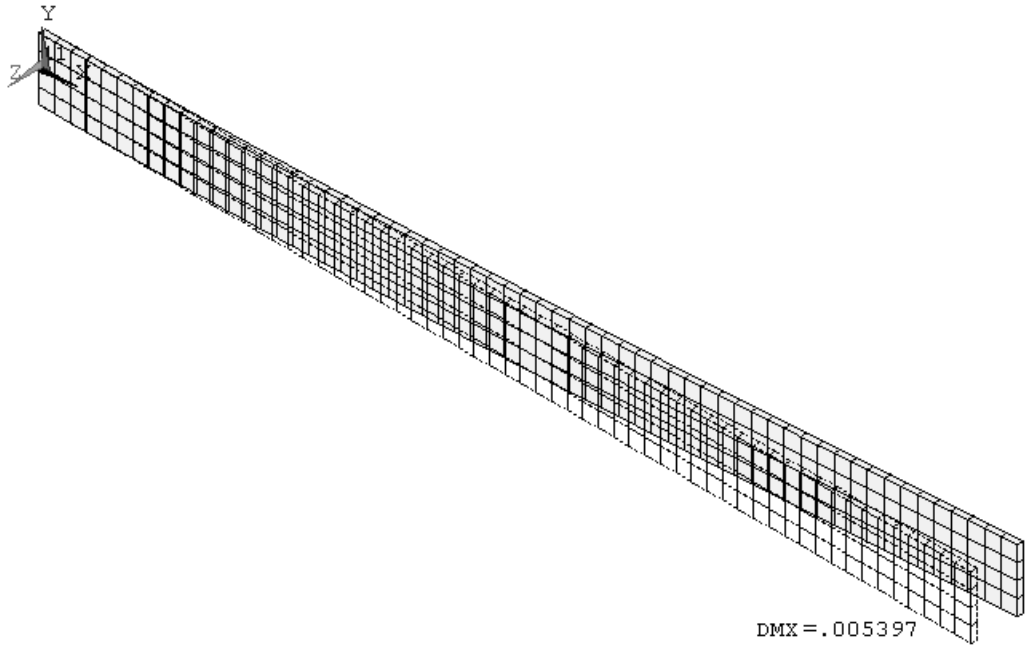

Figure 3.4 Deformed and undeformed states of the fixed-free untwisted beam

Finite element model of the pretwisted beam with smart patch under tip load acting in local z direction is shown in Figure 3.5. Piezoelectric layer shown in Figure 3.5 with light color is meshed by SOLID5 with the following mesh parameters:

- Number of elements in x direction = 5,
- Number of elements in y direction = 4,
- Number of elements in z direction = 1.

The piezoelectric patch has the following geometrical properties:

- Breadth b_p = 20 mm,
- Length s_p = 25 mm,
- Thickness t_p = 1 mm,
- Distance from the fixed support d_p = 10 mm

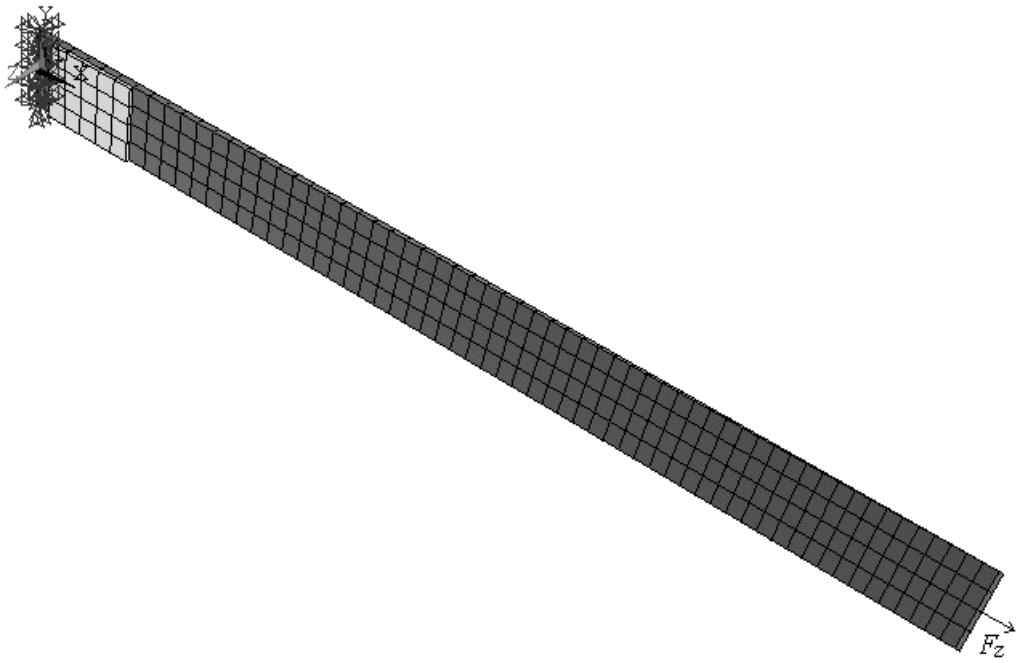

Figure 3.5 Finite element model of the pretwisted beam with smart patch

The material of piezoelectric patch is PZT-5H. Its material properties are given by Auld (1973) as follows:

Elements of mechanical compliance matrix:

$s_{11} = 16.5\ 10^{-12}\ m^2/N$

$s_{12} = -4.78\ 10^{-12}\ m^2/N$

$s_{13} = -8.45\ 10^{-12}\ m^2/N$

$s_{22} = s_{11}$

$s_{23} = s_{13}$

$s_{33} = 20.7\ 10^{-12}\ m^2/N$

$s_{44} = 43.5\ 10^{-12}\ m^2/N$

$s_{55} = s_{44}$

$s_{66} = 2\ (s_{11}-s_{12})$

Elements of piezoelectric strain matrix:

$d_{13} = -274\ 10^{-12}$ C/N

$d_{23} = d_{13}$

$d_{33} = 593\ 10^{-12}$ C/N

$d_{24} = d_{15}$

$d_{15} = 741\ 10^{-12}$ C/N

Elements of relative permittivity matrix under constant strain condition:

$\varepsilon_{11}^{S} / \varepsilon_0 = 1700$

$\varepsilon_{22}^{S} / \varepsilon_0 = 1700$

$\varepsilon_{33}^{S} / \varepsilon_0 = 1470$

where $\varepsilon_0 = 8.854\ 10^{-12}$ F/m is the free-space permittivity.

The order of the piezoelectric material matrix elements are based on IEEE standards, namely in the order *x*, *y*, *z*, *yz*, *xz*, *xy*. However, ANSYS input order is *x*, *y*, *z*, *xy*, *yz*, *xz*. Therefore, the matrices are needed to arrange for the ANSYS input by switching the shear terms (ANSYS. 2009).

To verify the finite element model of piezoelectric patch bonded to pretwisted beam, converse piezoelectric effect given in Equation (2.9) can be used, since analytical solution of the pretwisted beam with piezoelectric layer is not found in the published literature. Thus, a planar form of piezoelectric patch is modeled by SOLID5 elements by neglecting the twist of the patch due to the closeness of its position to fixed end. It has the following geometrical properties:

- Breadth b_p = 20 mm,
- Length s_p = 25 mm,
- Thickness t_p = 1 mm.

Finite element model of the planar form of piezoelectric patch with fixed-free boundary conditions and under electrical field is shown in Figure 3.6.

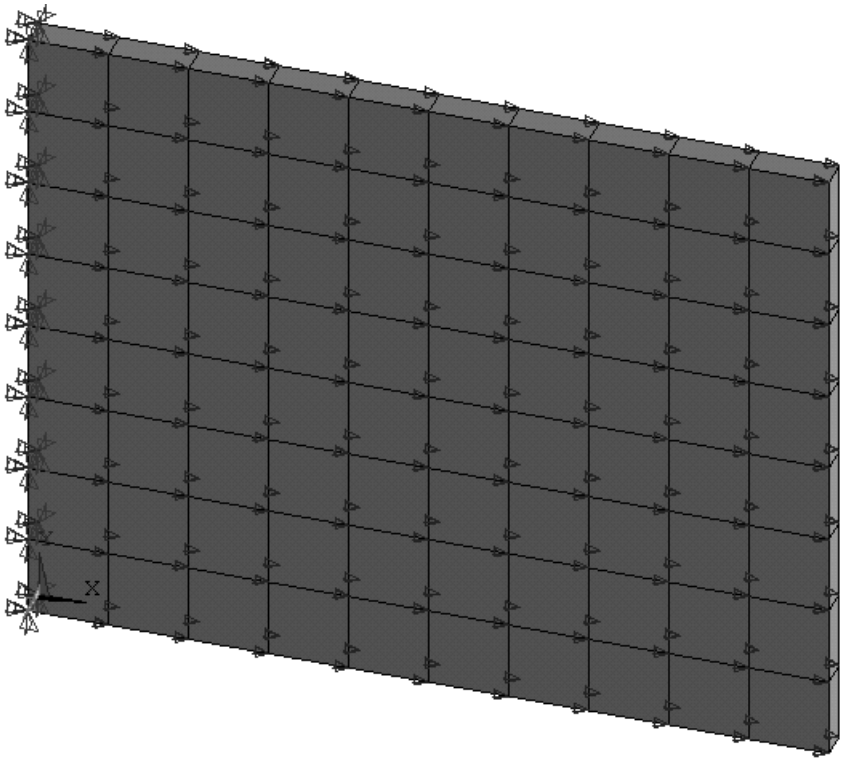

Figure 3.6 Finite element model of the planar form of piezoelectric patch

Analytical values of strains in x and z directions are calculated as S_1 and S_3, respectively, below:

$$S_1 = d_{13} E_3 = d_{13} \frac{-\Delta V}{t_p}$$
$$= -274.10^{-12} \frac{-200}{1.10^{-3}}$$
$$= 0.548\,10^{-4}$$

$$S_3 = d_{33} E_3 = d_{13} \frac{-\Delta V}{t_p}$$
$$= 593.10^{-12} \frac{-200}{1.10^{-3}}$$
$$= -0.1186\,10^{-3}$$

Finite element model results as contours of strains in *x* and z directions are shown in Figures 3.7 and 3.8, respectively. It can be seen from figures that analytical results are within the range of scales of which colors occupy the majority of the areas.

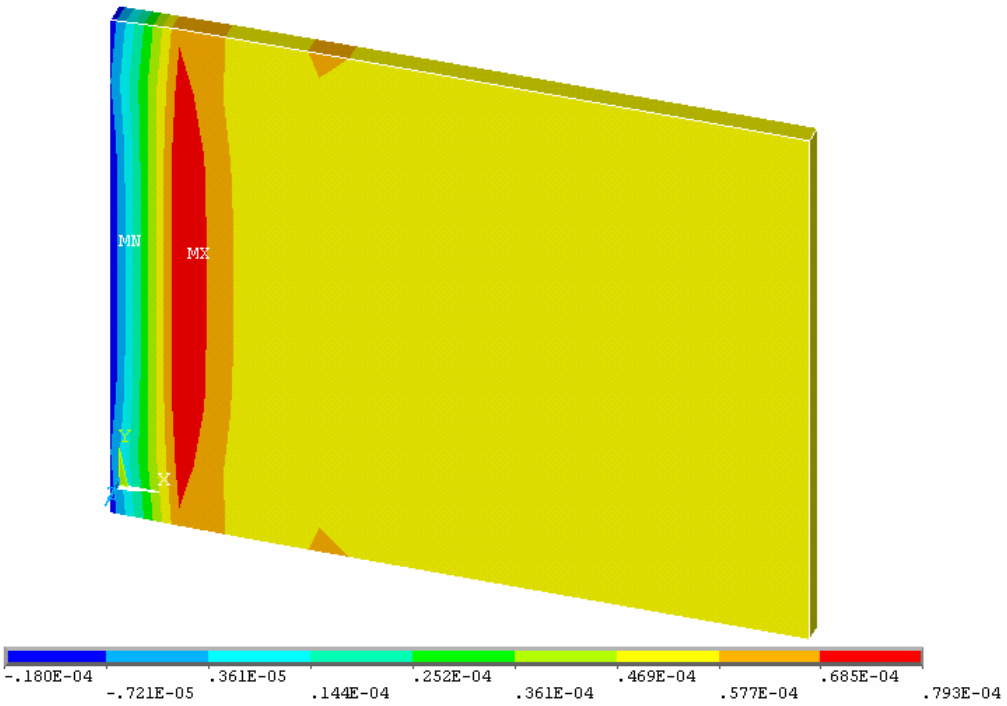

Figure 3.7 Contours of strains in *x* direction

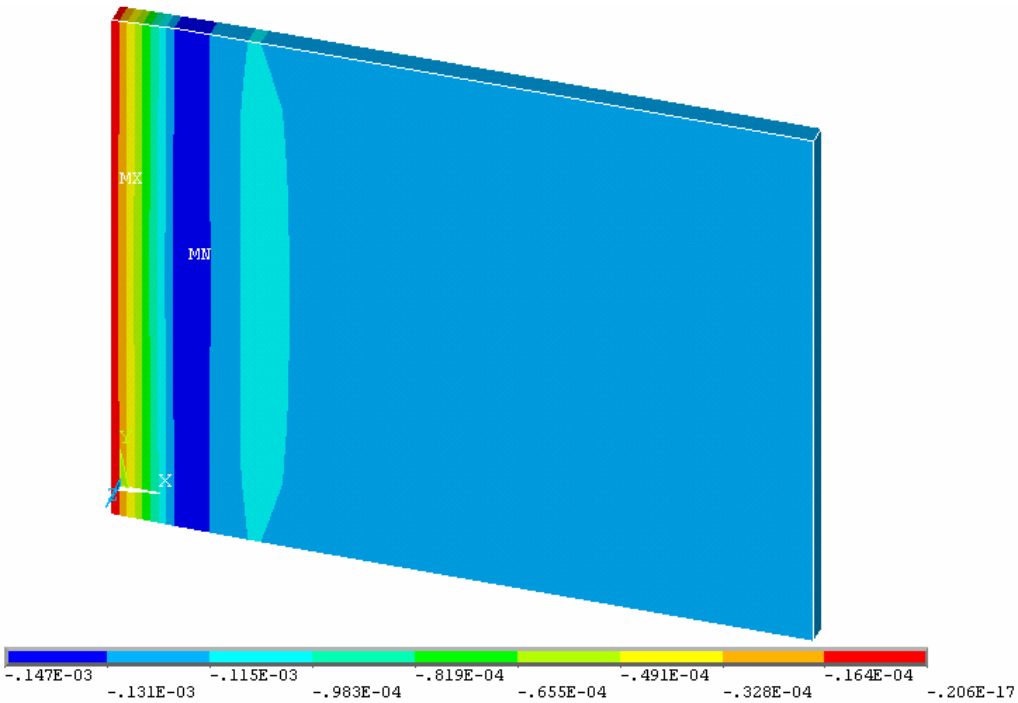

Figure 3.8 Contours of strains in *z* direction

3.2. Case Studies

Finite element model of the pretwisted beam with smart patch shown in Figure 3.5 is considered. As seen from Figure 3.5, it has fixed–free boundary condition and a tip load acting in local *z* direction. Local coordinates is the principle coordinates of the cross-section introduced in Figure 2.1. Tip load is used to get the voltage from the back and front surfaces of the piezoelectric patch. To determine the allowable tip load depending on the strength of aluminum and PZT, stress analysis is performed in first step considering the unit load.

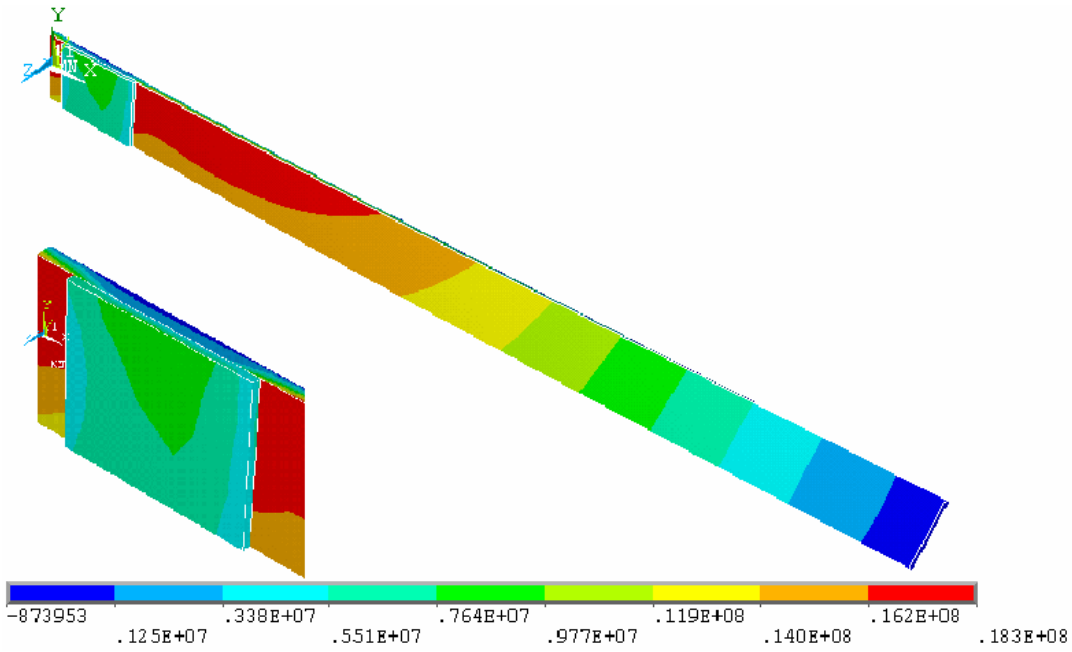

Figure 3.9 Principle stress contours

The yield stresses of aluminum can be taken as 250 MPa. Also, Weibull characteristic strength of PZT-5H is given by Anton et al (2012) as 115 MPa. It can be seen from Figure 3.9 that maximum principle stress in beam and PZT are 18.3 MPa and 9.77 MPa, respectively. Therefore, the limit tip load for each part can be calculated as

For Aluminum: $F_{zmaz-Al} = 250/18.3 = 13.66$ N

For PZT-5H: $F_{zmaz-PZT5H} = 115/9.77 = 11.77$ N

Therefore, assuming the safety factor as approximately 4, as tip load, 3 N can be applied to pretwisted beam. However, electromechanical analysis results of current studies are presented in the next figures for unit load.

Deformed and undeformed configurations of smart pretwisted beam are shown in Figure 3.10. Displacement of the beam is consistent with the applied load.

Contours of electric field of smart pretwisted beam in *z* direction are illustrated in Figure 3.11. It can be seen from figure that the maximum value of electrical field in *z* direction is 76200 V/m.

The zoomed view of piezoelectric patch showing contours of electric field in *z* direction are also given in Figure 3.12.

Due to the operating mode of piezoelectric patch used in this structure, strain distributions of PZT patch in *x* direction are presented in Figure 3.13.

In addition to presented plots, the stress contours of PZT patch in *x* direction are shown in Figure 3.14.

Moreover, to determine effects of the pretwist angle on electric field, variations of electric field from θ=5º to 75º are given in Figures 3.15-3.22.

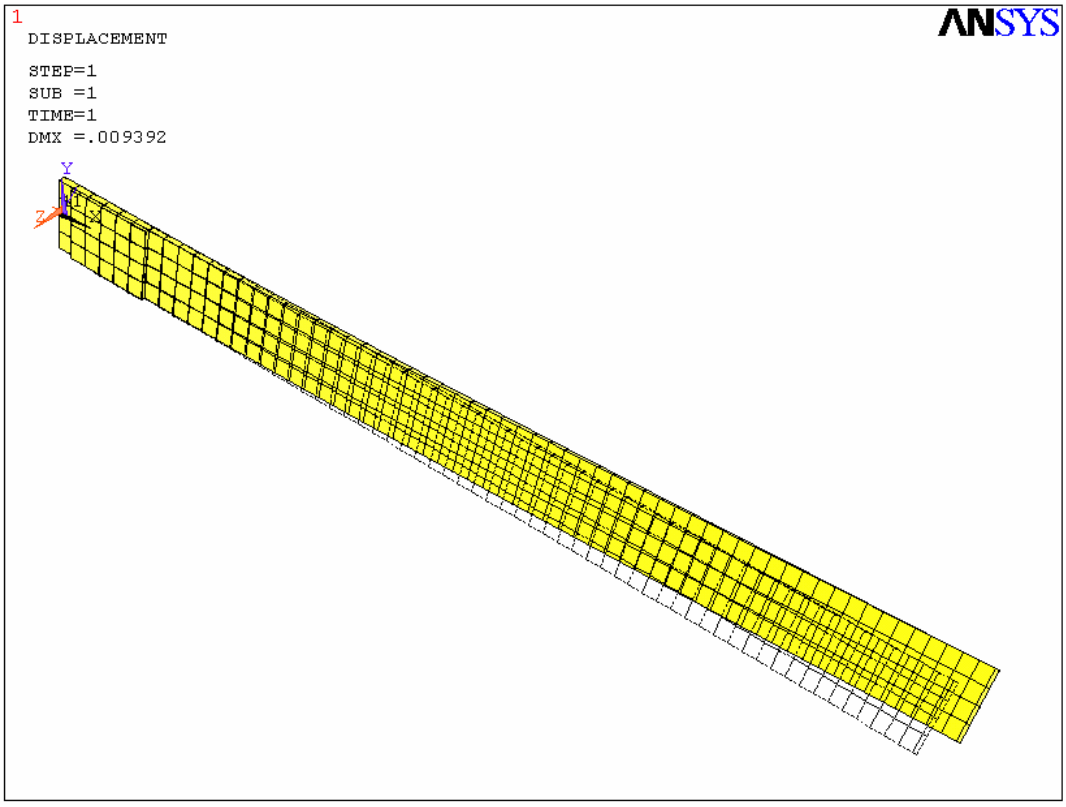

Figure 3.10. Deformed and undeformed configurations of smart pretwisted beam

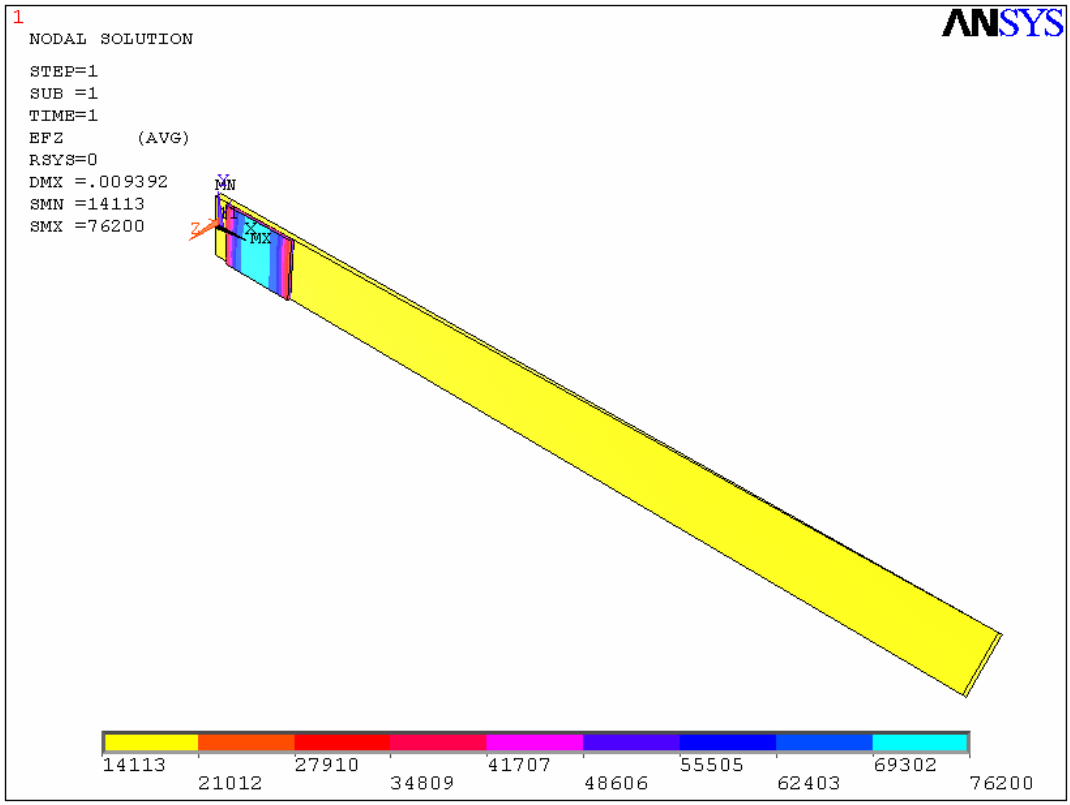

Figure 3.11. Contours of electric field of smart pretwisted beam in *z* direction

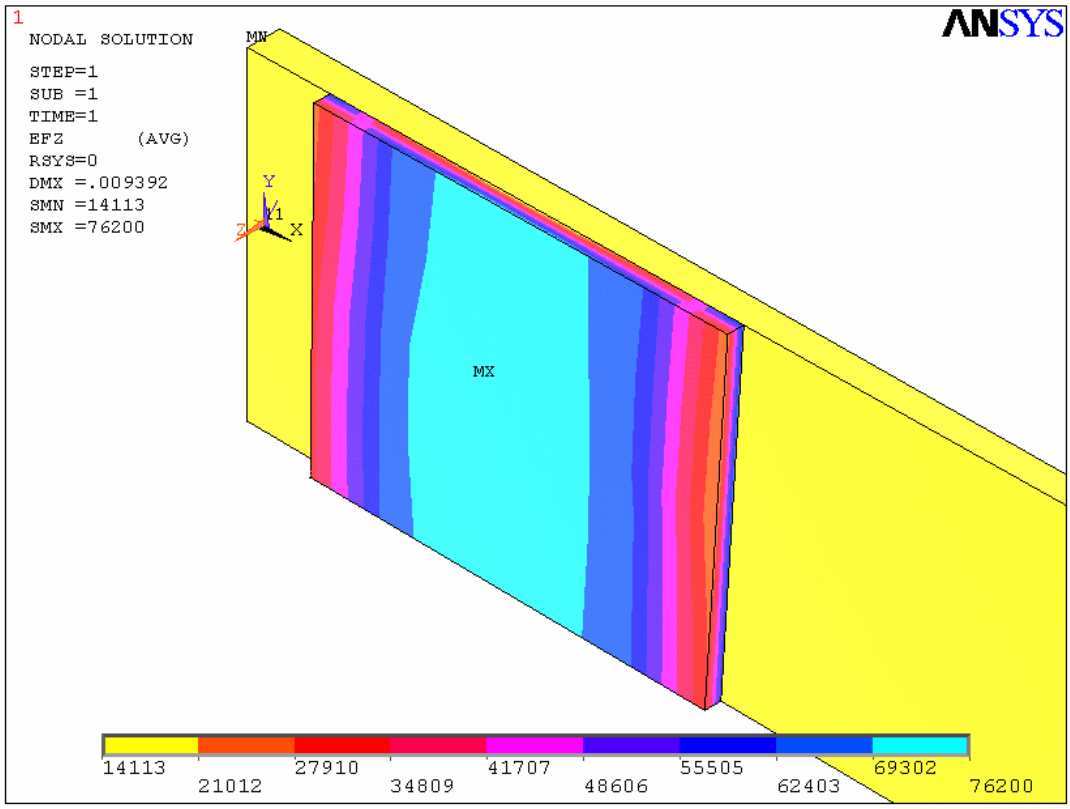

Figure 3.12. Electric field of PZT patch in *z* direction

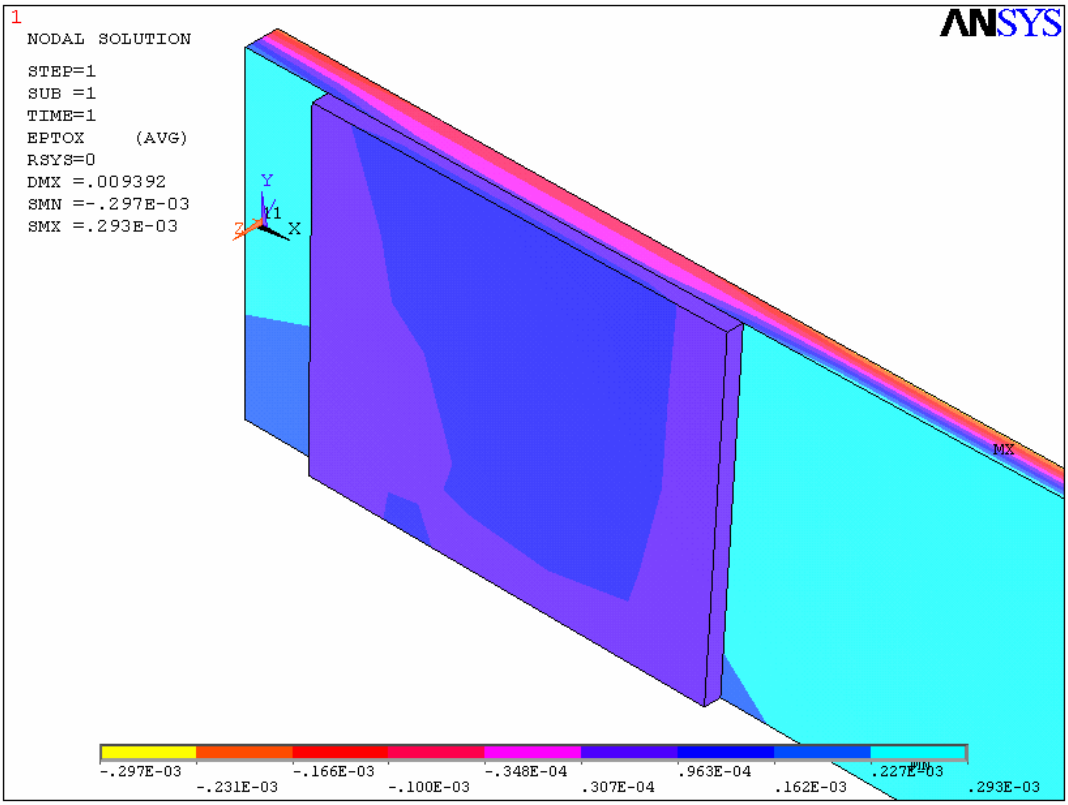

Figure 3.13. Strains of PZT patch in *x* direction

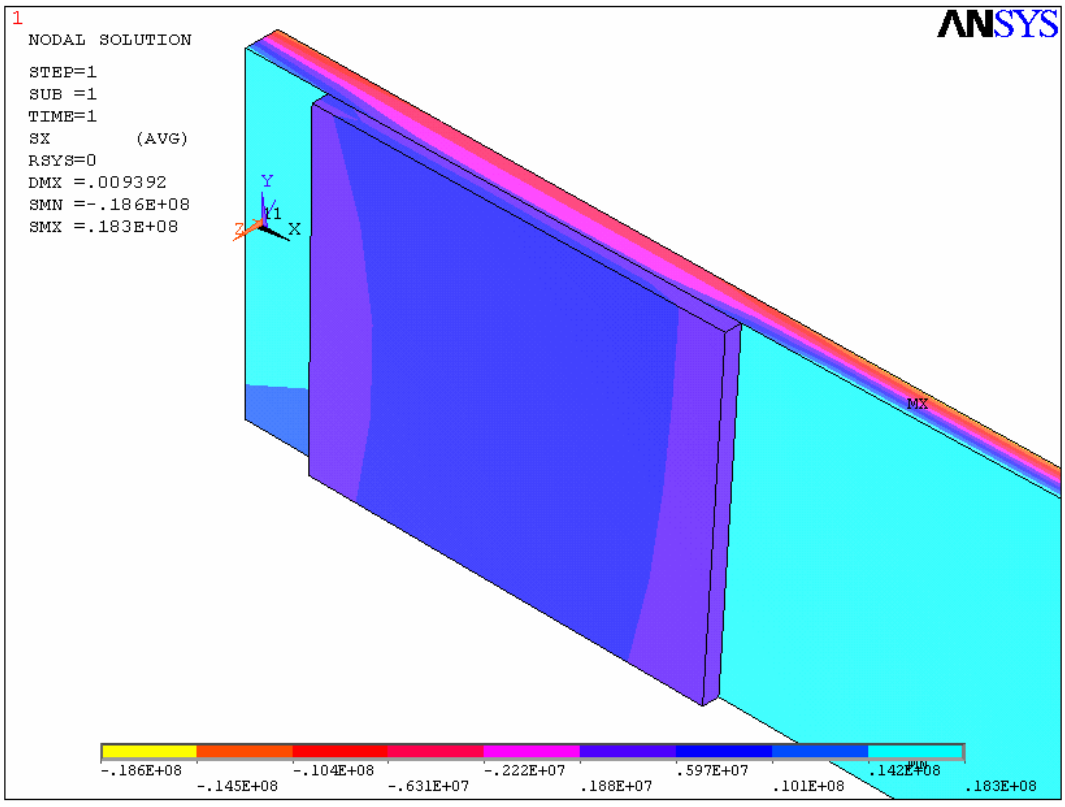

Figure 3.14. Stresses of PZT patch in *x* direction

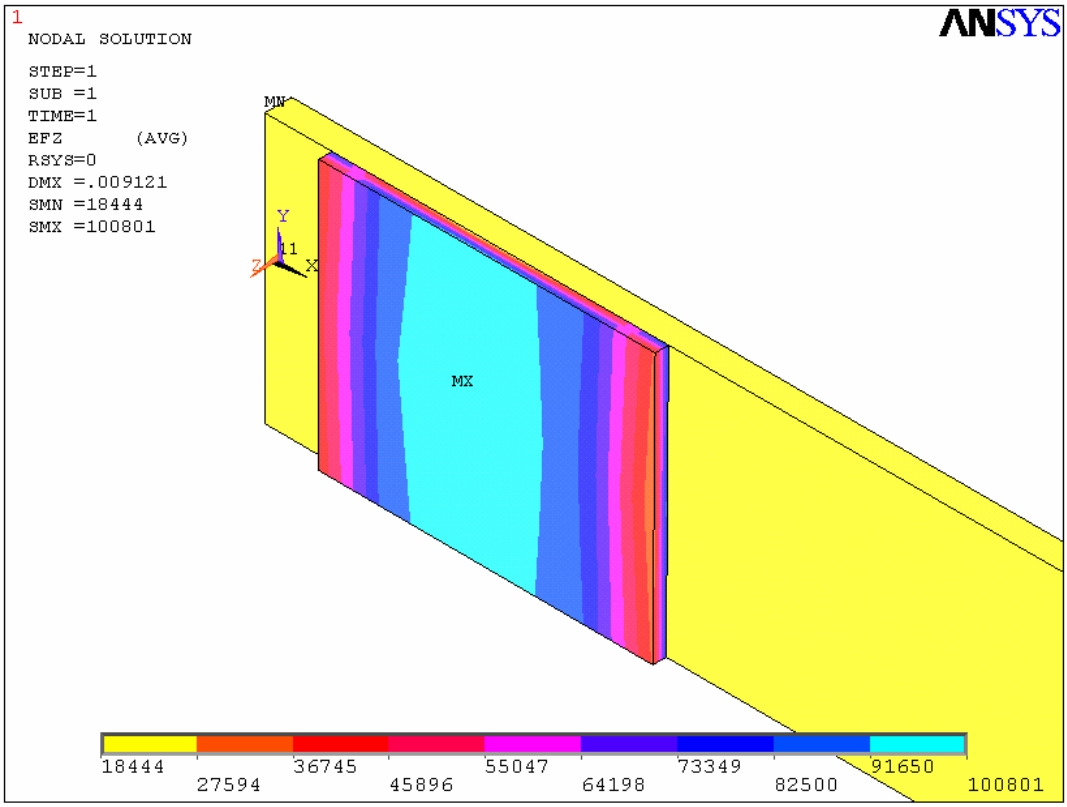

Figure 3.15. Electric field of PZT patch in z direction for θ=5º

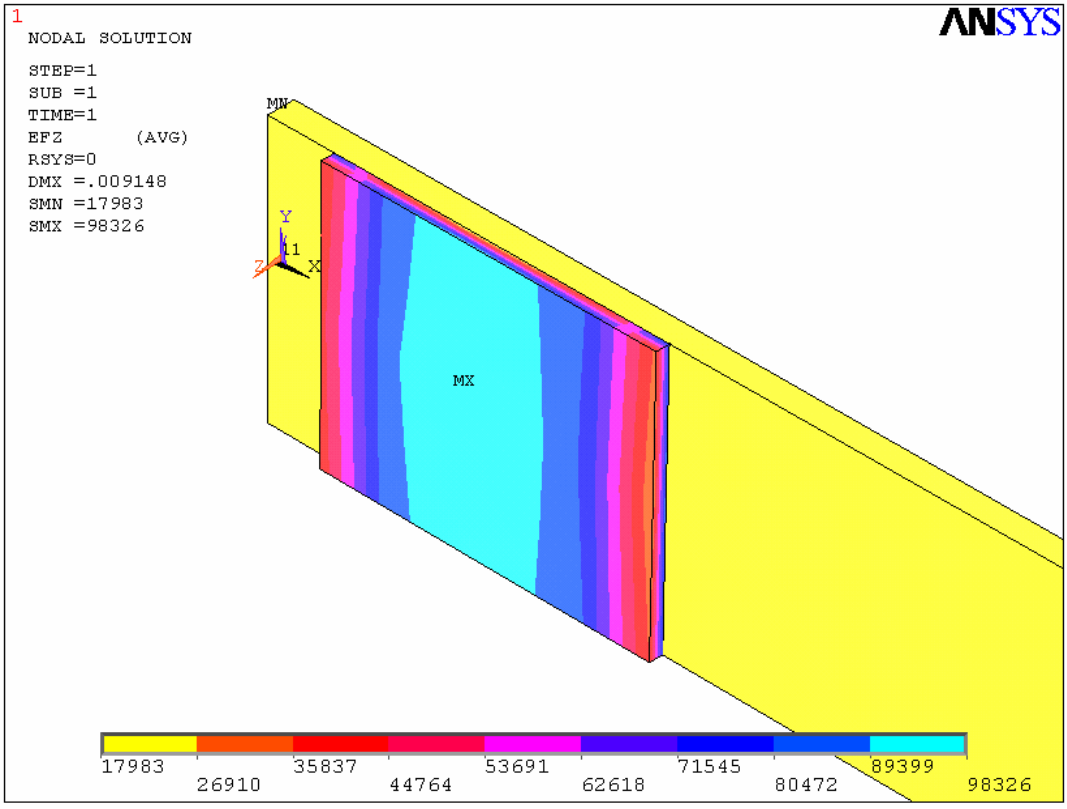

Figure 3.16. Electric field of PZT patch in z direction for θ=15º

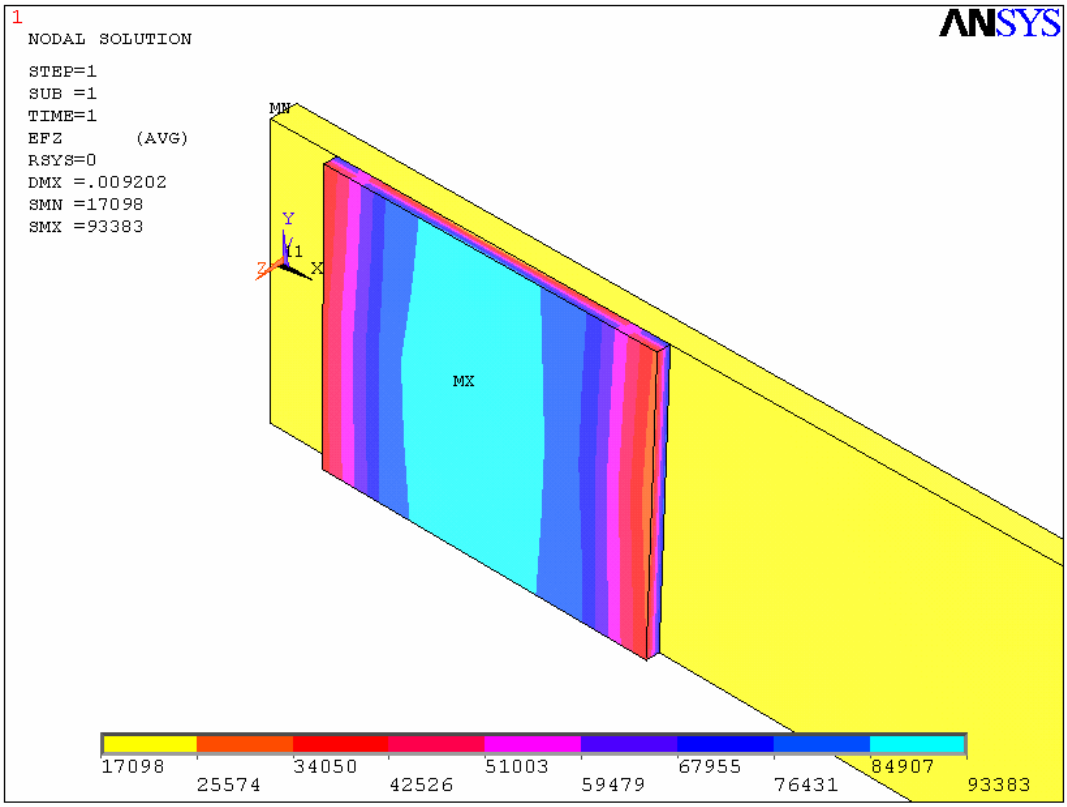

Figure 3.17. Electric field of PZT patch in *z* direction for θ=25º

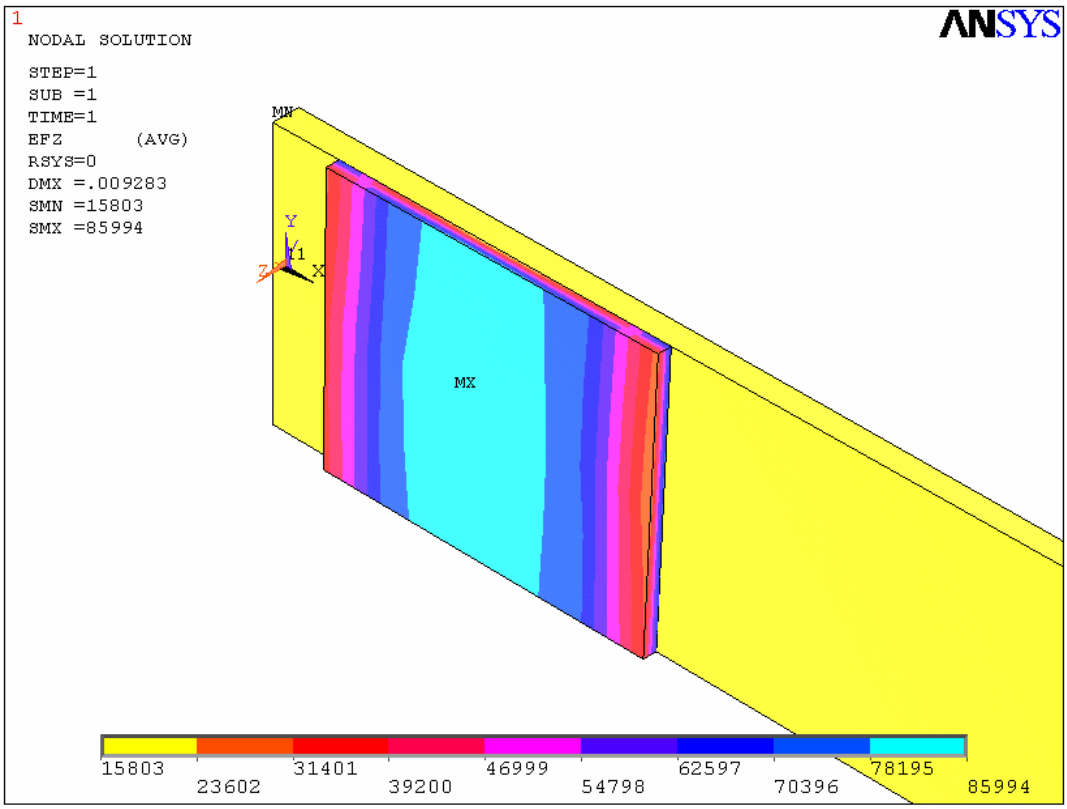

Figure 3.18. Electric field of PZT patch in *z* direction for θ=35º

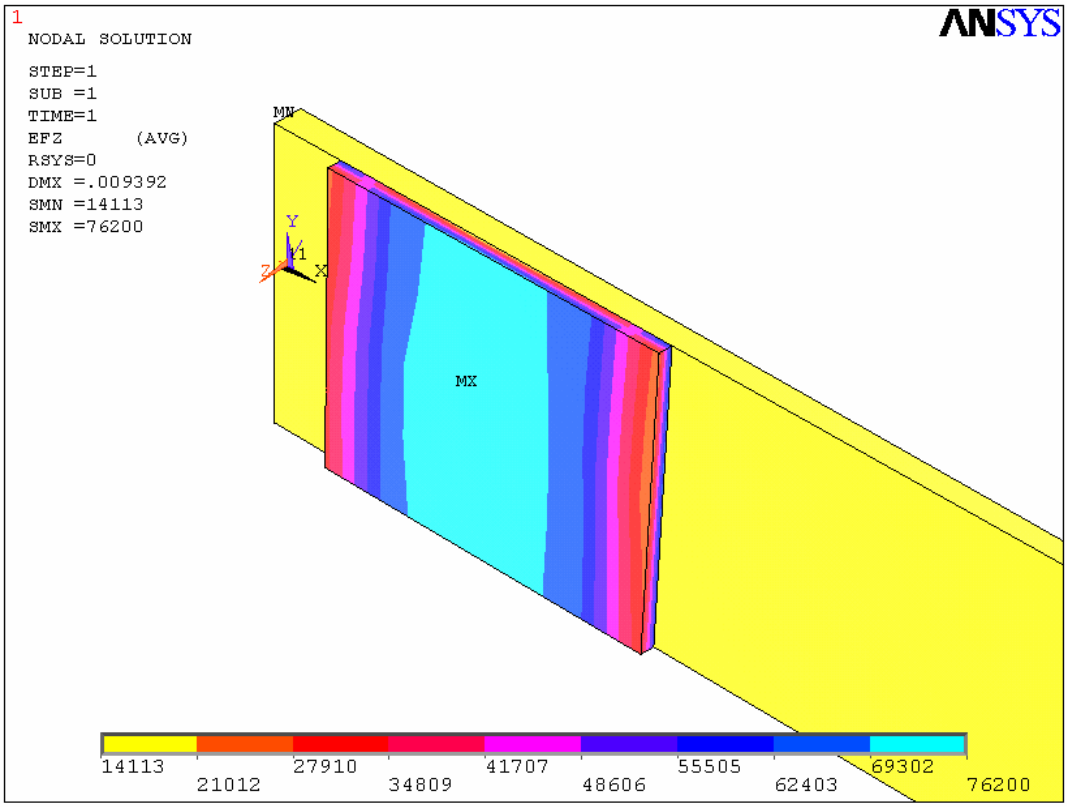

Figure 3.19. Electric field of PZT patch in *z* direction for θ=45º

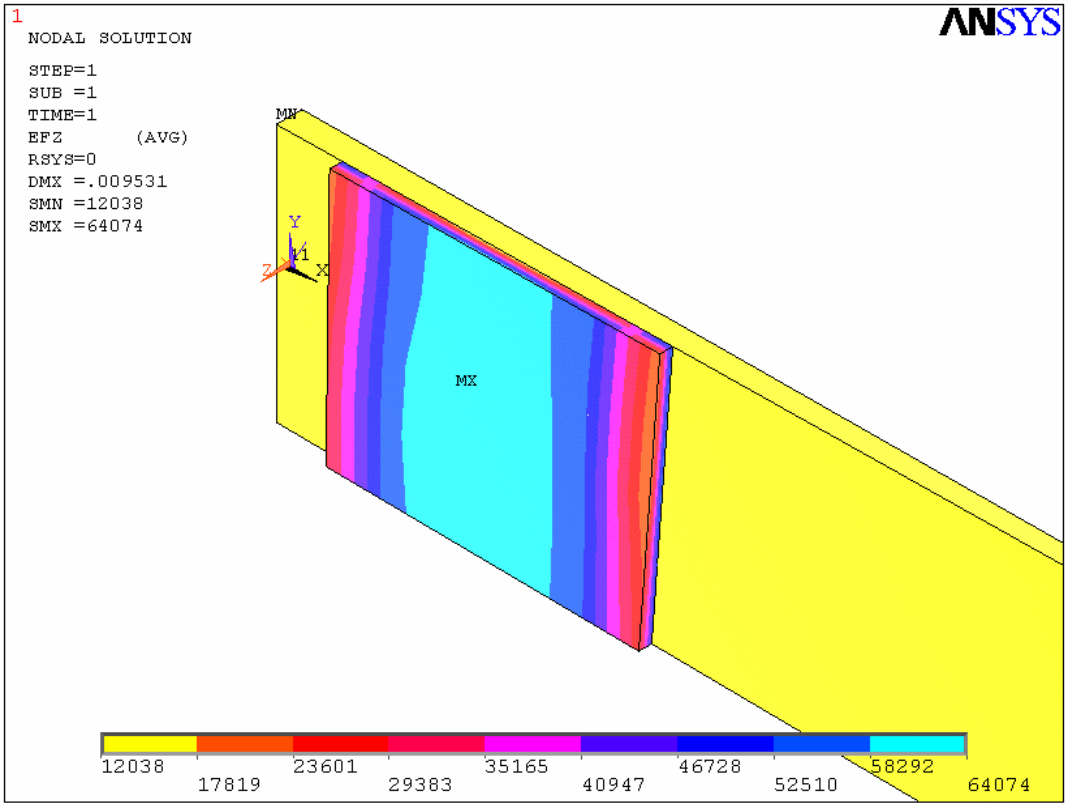

Figure 3.20. Electric field of PZT patch in *z* direction for θ=55º

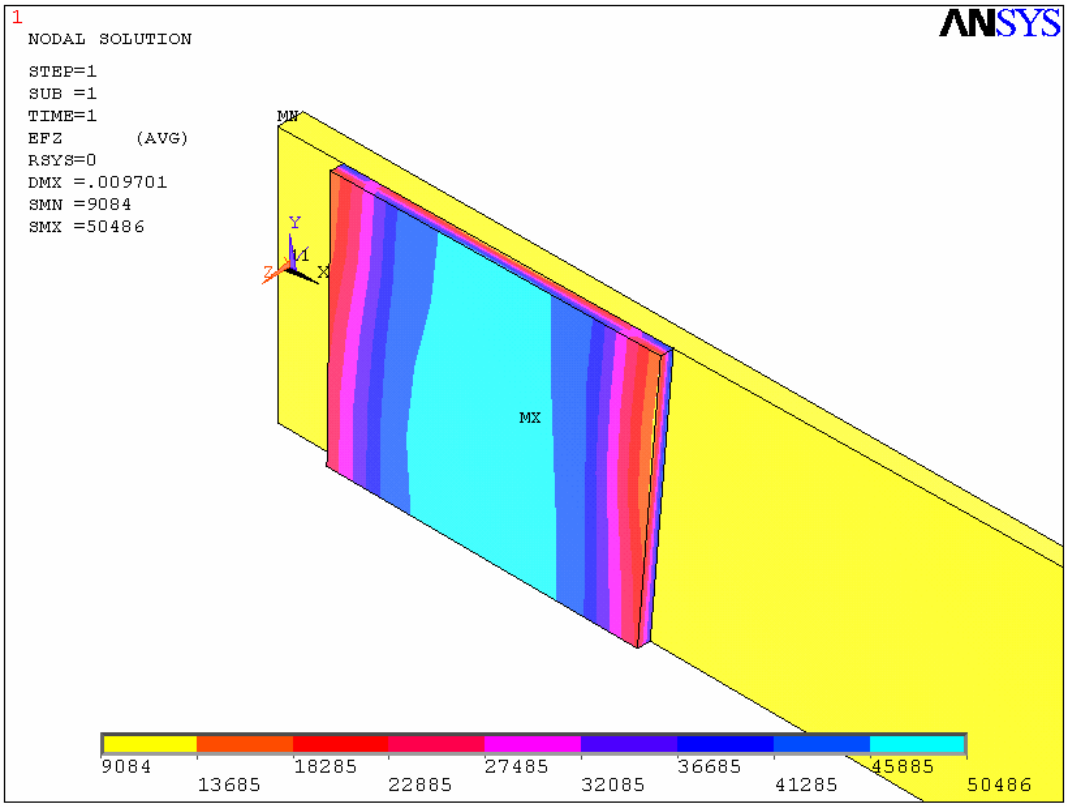

Figure 3.21. Electric field of PZT patch in *z* direction for θ=65º

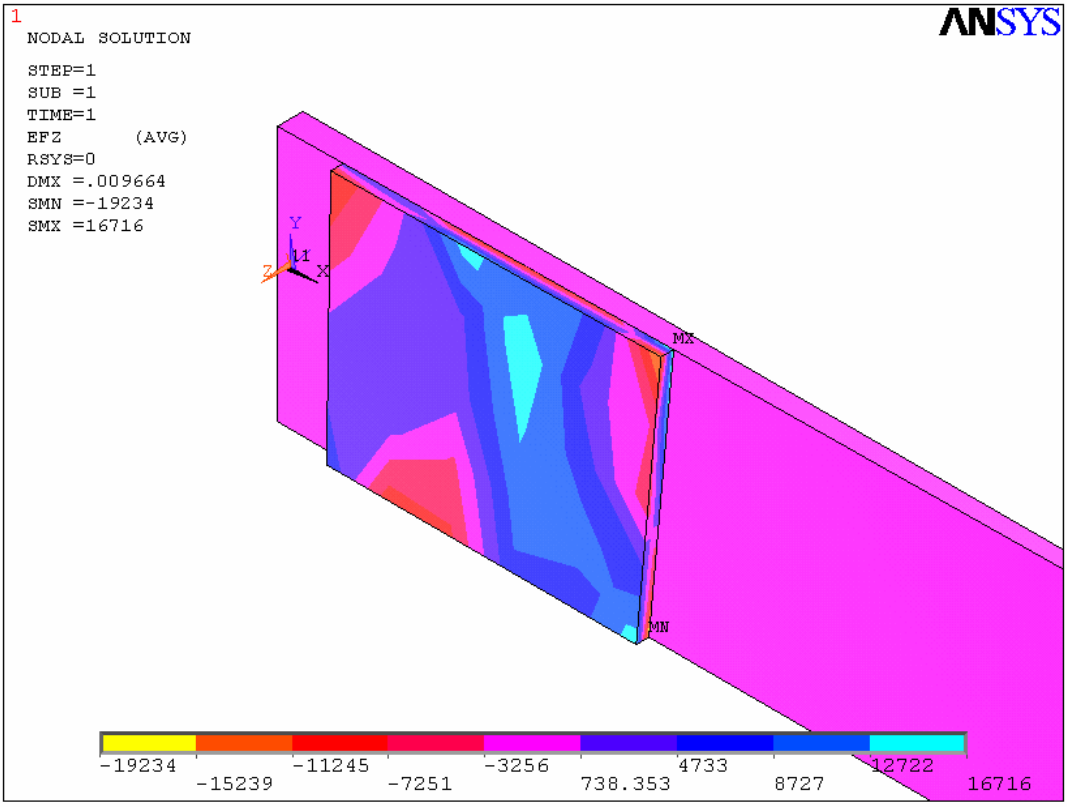

Figure 3.22. Electric field of PZT patch in *z* direction for θ=75º

Variation of electric field depending on the pretwist angle is plotted by using the results given in Figures 3.15-3.22.

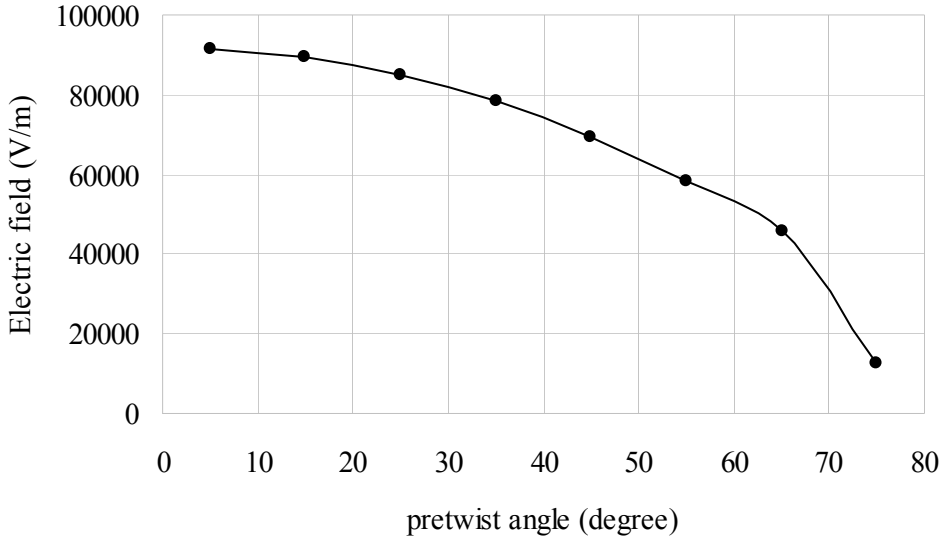

Figure 3.23. Plot of Electric field versus twist angle

Simple tests for piezoelectric effects are illustrated in Appendix A.

3.3. Discussion of Results

A computer program developed in ANSYS by using APDL (ANSYS Parametric Design Language) is proved considering the following items:

- the deformed configuration and its numerical value,
- the strain distributions along the beam,
- the voltage generation on piezoelectric patch.

The effects of the pretwist angle on electric field are analyzed. When the pretwist angle is increased, strain in *x* direction is reduced. Therefore, the value of electric field is decreased. The reason of these results is the direction of the tip load which is applied in local *z* direction.

CHAPTER 4

CONCLUSIONS

Modeling and analysis of uniform straight beams with piezoelectric layers are common in the existing literature. However, when the beam has pretwist, analysis of this type of smart beams require numerical methods.

Modeling and analyses of pretwisted beams having piezoelectric smart materials are acomplished by using ANSYS Mechanical. Instead of usage of graphical user interface, APDL (ANSYS Parametric Design Language) in ANSYS is used to code a parametric program.

The effects of the pretwist angle on electric field are analyzed. It is shown that when the pretwist angle is increased, the value of electric field due to the load acting in local z direction is decreased.

REFERENCES

ANSYS, 2009. Coupled-Field Analysis Guide, Release 10.0, Canonsburg: ANSYS, Inc.

Anton, S.R., Erturk, A., and Inman, D.J., 2012. Bending strength of piezoelectric ceramics and single crystals for multifunctional load-bearing applications. *IEEE Transactions on Ultrasonics, Ferroelectrics, and Frequency Control* 59: 1085-1092.

Allik, H., and Hughes, T.J.R. 1970. Finite element method for piezoelectric vibration, *International Journal for Numerical Method in Engineering* 2: 151-7.

Bailey, T., and Hubbard, J., 1985. Distributed Piezoelectric-Polymer Active Vibration Control of a Cantilever Beam. *Journal of Guidance, Control, and Dynamics* **8**(5): 605–611.

Cesnik, C.E. and Morales, M.O., 2001. Active beam cross-sectional modeling, *Journal of Intelligent Material Systems and Structures* 12: 483-496.

Choi, S.C., Park, J.S., and Kim, J.H., 2007. Vibration control of pre-twisted rotating composite thin-walled beams with piezoelectric fiber composites, *Journal of Sound and Vibration* 300: 176–196.

Crawley, E.F. and de Luis, J. 1987. Use of piezoelectric actuators as elements of intelligent structures. *AIAA Journal* **25:** 1373–1384.

Cook, R.D, Malkus, D.S., and Plesha, M.E., 1989. Concepts and Applications of Finite Element analysis. New York: John Wiley and Sons, Inc.

Fu, C.C., 1974. Computer analysis of a rotating axial-turbomachinary blade in coupled bending-bending-torsion vibrations, *International Journal for Numerical Methods in Engineering* 8: 569-588.

Ganguli, R., Dipali, T., and Viswamurthy, S.R., 2016. Smart Helicopter Rotors Optimization and Piezoelectric Vibration Control, Switzerland: Springer.

Houbolt, J.C. and Brooks, G.W. 1958. Differential equations of motion for combined flapwise bending chordwise bending and torsion of twisted nonuniform rotor blades. *NACA Report* 1346.

IEEE, 1988, IEEE Standard on Piezoelectricity, Std. 176-1987, Piscataway, New Jersey: IEEE.

Kiral, Z. Malgaca, L., and Akdag, M. 2008. Active control of residual vibrations of a cantilever smart beam, *Turkish Journal of Engineering Environmental Science* 32: 51–57.

Kohnke, P., 2004. ANSYS, Inc. Theory Reference. Canonsburg: ANSYS, Inc. online documentation or the ANSYS

Leo, D.J., 2007. Engineering Analysis of Smart Material Systems, New Jersey: John Wiley & Sons, Inc.

Liu, K.C., Friend, J., and Yeo, L., 2007. Vibration analysis of pretwisted beams for the design of hybrid axial-torsional transducers, 48th AIAA/ASME/ASCE/ AHS/ASC Structures, Structural Dynamics, and Materials Conference, Honolulu, Hawaii.

Montoya, J., 1966. Coupled bending and torsional vibrations in a twisted rotating blade, *The Brown Boveri Review* 53: 216-230.

Petyt, M., 2010. Introduction to Finite Element Vibration Analysis. Cambridge: Cambridge University Press.

Preumont, A., 2002. Vibration Control of Active Structures. New York: Springer-Verlag.

Reddy, J.N., 1993. An introduction to the finite element method. Second edition. New York: McGraw-Hill.Inc.

Shete, C. D., Chandiramani, N. K., and Librescu, L.I., 2007. Optimal control of a pretwisted shearable smart composite rotating beam, *Acta Mechanica* 191: 37–58.

Smith, R.C., 2005. Smart Material Systems: Model Development. Philadelphia, PA: SIAM.

Song, O., Oh, S.Y., and Librescu, L., 2002. Dynamic behavior of elastically tailored rotating blades modeled as pretwisted thin-walled beams and incorporating adaptive capabilities, *International Journal of Rotating Machinery* 8(1): 13-25.

Valliappan V. Harursampath, D., Roy, S., and Yu, W., 2014. Variational asymptotic modelling of an initially-curved and pre-twisted smart beam, 22nd AIAA/ASME/AHS Adaptive Structures Conference, National Harbor, Maryland.

Wang , J., Li, D., and Jiang, J., 2015. Coupled flexural–torsional vibration of spinning smart beams with asymmetric cross sections, Finite Elements in Analysis and Design 105: 16–25.

Yardimoglu, B., 2015. Lecture notes on Finite Element Method, Izmir: Izmir Institute of Technology.

Yardimoglu, B., 2016. Lecture notes on Advanced Mechanics of Materials, Izmir: Izmir Institute of Technology.

Yardimoglu, B. and Inman, D.J., 2004. Coupled bending-bending-torsion vibration of a rotating pre-twisted beam with aerofoil cross-section and flexible root by finite element method. *Shock and Vibration* 11: 637-646.

Yardimoglu, B. and Yildirim, T., 2004. Finite element model for vibration analysis of pretwisted Timoshenko beam, *Journal of Sound and Vibration* 273: 741-754.

APPENDIX A

EXPERIENCE WITH PIEZOELECTRIC MATERIAL

First experience is obtained by using piezo buzzer with led. The piezo buzzer is supported as seen in Figure A.1. Then, a transverse load is applied from the center of the piezo buzzer as illustrated in Figure A.2. Therefore, the led lights up.

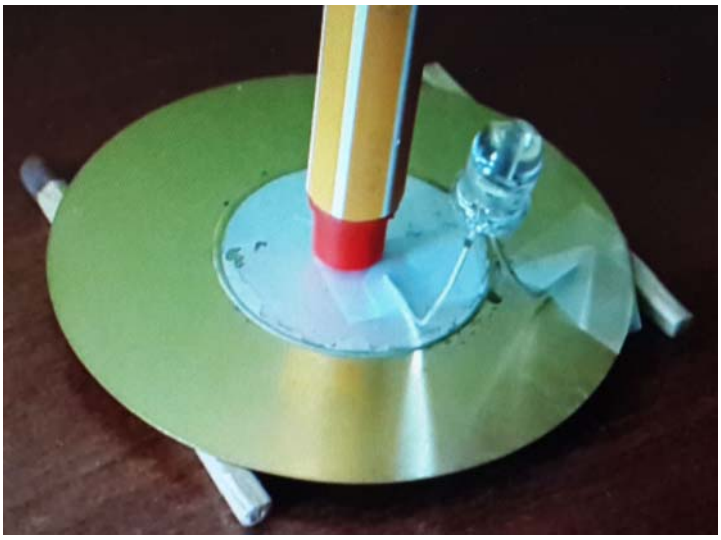

Figure A.1. Pizeo buzzer and led without load.

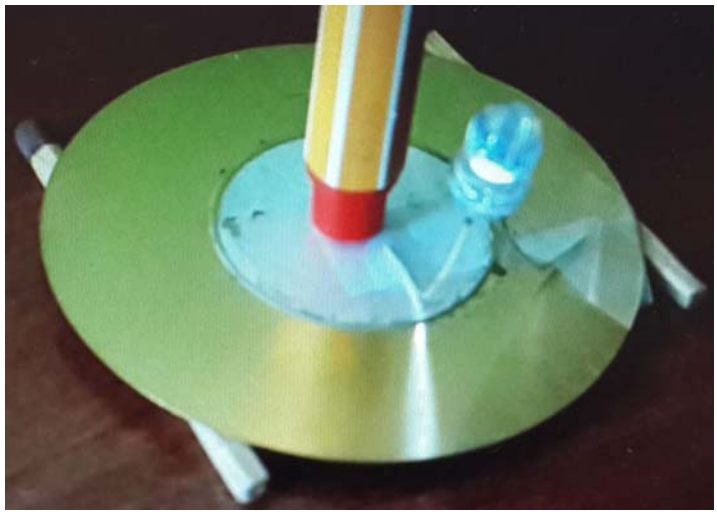

Figure A.2. Pizeo buzzer and led with load.

Second experience is gained by using piezo buzzer and digital multimeter. The piezo buzzer is supported as before as seen in Figure A.3. Then, a transverse load is applied from the center of the piezo buzzer. Therefore, 10.78 volt is read from the screen.

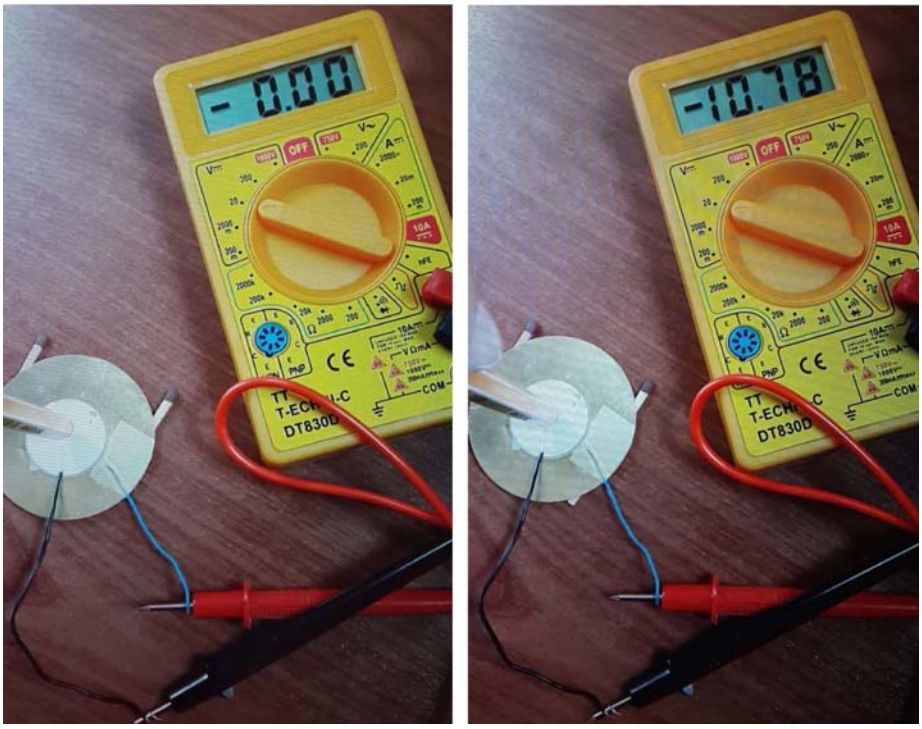

Figure A.3. Pizeo buzzer without and with load.